Fabrication of Size- and Shape- Controllable Mixed-Scale PDMS Channel Networks Including 3D Microfunnels

Yunjeong Lee
Department of Mechanical Engineering
Graduate School of UNIST
2015

Fabrication of Size- and Shape- Controllable Mixed-Scale PDMS Channel Networks Including 3D Microfunnels

Yunjeong Lee

Department of Mechanical Engineering
Graduate School of UNIST

Fabrication of Size- and Shape- Controllable Mixed-Scale PDMS Channel Networks Including 3D Microfunnels

A thesis submitted to
the Graduate School of UNIST
in partial fulfillment of
the requirements for the degree of
Master of Mechanical Engineering

Yunjeong Lee

01.09.2015
Approved by

Advisor:
Heungjoo Shin

Fabrication of Size- and Shape- Controllable Mixed-Scale PDMS Channel Networks Including 3D Microfunnels

Yunjeong Lee

This certifies that the thesis of Yunjeong Lee is approved

01.09.2015

Thesis Supervisor: Professor Heungjoo Shin

Thesis Committee Member: Professor Taesung Kim

Thesis Committee Member: Professor Jaesung Jang

ABSTRACT

In this thesis, a novel batch fabrication technology for a mixed-scale PDMS (Polydimethylsilane) channel networks using carbon- micro electromechanical systems (MEMS) and single molding process is introduced. Nanofabrication has been used in broad research fields including single electron memories, multiple tunnel junction (MTJ) devices, micro electromechanical systems (MEMS) sensors, and nanofluidic devices. Nanofluidic channel networks are crucial parts in various applications such as DNA electrophoresis, bio sensors, molecular preconcentration, ionic transport nanofluidic diodes, desalination, nanofludic transistors because of their unique phenomena including ion concentration polarization, ion rectification effect, nanocapillarity and electrical double layer overlap. However, the research on the nanofluidics has been limited because of the lack of simple and cost-effective nanofabrication technologies. Microfabrication technologies that are compatible with nanofabrication processes also needs to be developed so as to integrate microfluidic channels with nanochannels, because the microchannels guide sample fluid into and out of the nanochannels and thus mixed-scale channel networks are the basic architecture of the nanofluidic devices. However, the fabrication of mixed-scale channel networks is limited by difficult alignment processes between nanostructures and microstructures, high fabrication cost, and time consuming and complex processes. These limitations can be overcame by utilizing carbon-MEMS technology and single polymer molding process.

A mixed-scale carbon structure as the mold of a Poly (dimethylsiloxane) (PDMS) channel network was fabricated using conventional UV lithography and pyrolysis. A single molding process using multi-layers of hard PDMS and soft PDMS completes the fabrication of mixed-scale PDMS channel networks including 55-nm-high and 441-nm-wide nanochannels. The quality of the PDMS molding process was evaluated using a scanning

electron microscope (SEM) and an atomic force microscope (AFM). The surface energy of the pyrolyzed carbon mold could be modulated by controlling pyrolysis temperature resulting in high surface energy. As a result, a single carbon mold could replicate PDMS channel networks more than 40 times without anti-adhesion coating. The hermetic sealing and uniformity of the PDMS nanochannel were evaluated by filling the mixed-scale PDMS channel networks with fluorescein isothiocyanate (FITC). The properties of PDMS nanochannels were characterized by measuring I-V relationship in KCl solution. Except for the simple fabrication of the complex carbon mold, the pyrolysis process also enabled the formation of smoothly tapered mold side wall because of good adhesion between the photoresist and substrate, and volume reduction in pyrolysis. As a result, 3-D funnels could be integrated at the entrance and exit of the nanochannel. By this novel 3-D funnel structure, efficient entrapment of a single micro particle at the entrance of a nanochannel was enabled. It is expected that the mixed-scale PDMS channel networks with 3D-funnels can be applied to nanoelectroporation for efficient cell transfection.

DEDICATION

This thesis is lovingly dedicated to my parents, Seungyeon Lee and Geumok Seo, for their support, sacrifice and love throughout my life.

LIST OF FIGURES

Figure 4.9 Optical microscopy images of the mixed-scale PDMS channel network including 3-D funnels, micro-nanochannels, nanochannels and trapped 1-μm-diameter micro particles. (a-b) Single entrapment of micro particles with microfunnels with 30^{o} of entrance angle and 15μm in height. (c-f) Entrapment of multiple micro particles at 3-D funnels with wide and short entrance.

LIST OF TABLES

CONTENTS

1

Introduction

In this chapter, a background for fabrication technologies, applications for the mixed-scale channel networks will be introduced. Also, the simple overview of this thesis will be given.

1 Introduction

1.1 Background

Nanochannel is a nanoscale conduit that has characteristic dimension below 100-nm at least one side. The nanochannel shows the unique phenomena such as ion rectification [1], ion concentration polarization (ICP) [2-3], nanocapillarity [4], electrical double layer (EDL) overlap [5], etc. Unique characteristics are emerged due to the large surface effect of the nanochannel. Meanwhile, a nanopore is a nanoscale hole and used for analysis of nanoscale phenomena with the nanochannel. Usually, nafion membrane, silicon and graphene are used for nanopore [2]. Although nanopore has the advantages including the simple, easy fabrication and similarity with ionic channel in the body, nanopore is insufficient for broad application such as a biosensor because of the impossibility of the pre-/ post-processing, large noise. On the other hand, nanochannel has enormous advantages such that nanochannel can be used to separate of the electric field and detect the biomolecules using small noise, pre-/ post-processing and single molecular sequential processing.

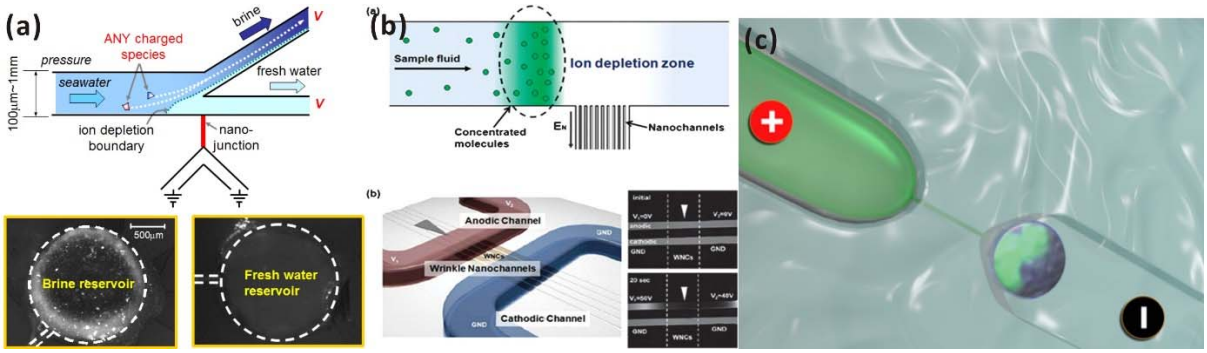

Figurer 1.1 Various applications of the nanofluidics; (a) Seawater desalination from Kim *et al.* (2010) [6], (b) Protein concentration in the wrinkled nanochannels (WNCs) from Chung *et al.* (2008) [8], (c) Schematic image of the nanoelectroporation from Boukany *et al.* [18].

There are plenty of applications using the nanofluidic channel devices based on their high surface effect and characteristic dimension shown by Figure 1.1. When the characteristic dimension of the channel is reduced around 100-nm, this length is similar to the electrical double layer and then the electrical double layer is overlapped in the narrow nanofluidic channel [5]. It causes ion concentration polarization in the nanochannel. Ion depletion zone and ion enrichment zone are formed across the nanochannel filled with an electrolyte solution such as potassium chloride (KCl) and sodium chloride (NaCl). Invaluable applications including the desalination [6], nanofluidic diode [7], biomolecule preconcentration [8-10] can be realized using ICP phenomenon in the nanofluidic device. Also, nanofluidic device can be applied to bio applications such as a bio sensing [11-12], biofilter [13-14], DNA stretching [15-17] and nanoelectroporation [18-19] that is a powerful tool for the cell transfection.

1.2 General Fabrication Techniques

The most popular lithography technology is UV lithography. Because UV lithography enables easy microfabrication, large area patterning throughout a wafer scale, patterning on the flexible substrate, and easy shape and dimension control. However, the resolution of UV lithography is limited up to ~1 μm due to a limitation of the diffraction of light. Therefore, UV lithography cannot be applied for the nanofabrication. A variety of nanofabrication techniques have been developed over 20 years including the electron beam lithography (EBL) [21-23], focused ion beam (FIB) milling [24-25] and nano imprint lithography (NIL) [26-29]. Nanofabrication techniques have evolved to reach lateral resolution of ~2 nm. Moreover, several unconventional fabrication techniques have been developed to overcome a limitation of the nanofabrication such as a high cost, long process time and difficult alignment with microstructures [30]. In this thesis, fabrication technologies

for a nanochannel are categorized as two types depending on their substrates including a hard and a soft materials.

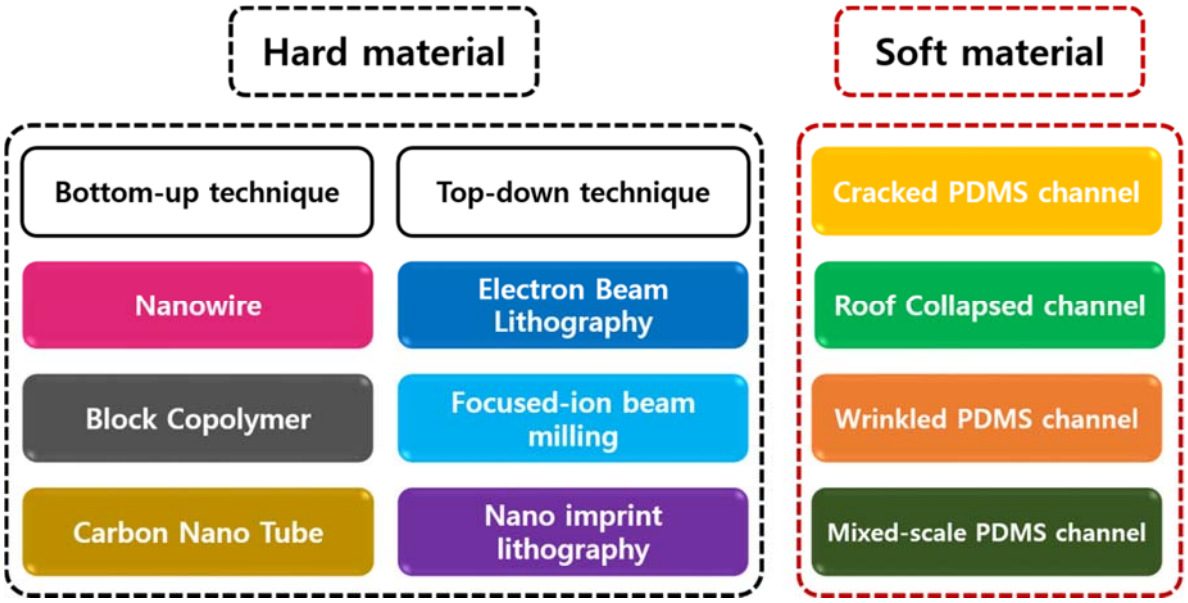

Figure 1.2 Categorization of the various nanofabrication technologies. Simply, the technologies can be divided by substrate materials including hard materials and soft materials.

1.2.1 Hard Materials

Some hard materials such as a quartz, Si and fused silica are useful for a nanofabrication to fabricate the nanopatterns because of a precise dimension control and less chance of a deformation. Flat and hard materials can be patterned using top-down and bottom-up approaches. Bottom-up approach starts from atomic scale and forms a designed structure by the synthesis. On the other hand, top-down approach starts from a bulk material and fabricates a designed structure through various removal techniques such as an etching [31], a lithography, an ion irradiation [32], etc. Bottom-up approach have the merits of an accurate size and shape control but requires more time to fabricate a structure than top-down

approach. Thus, top-down approach can fabricate more elaborate and various structures during short time than bottom-up approach. So, top-down approach is used in many research groups. A typical top-down approach is the electron beam lithography (EBL) shown by Figure 1.3 describing the nanofluidic device fabricated by the EBL. Uniform and very narrow nanochannels were fabricated by EBL. In EBL, an electron beam writes the nanopatterns directly on an electron beam resist spin-coated substrate. So nanostructure can be fabricated with various shapes without using a mask with a spatial resolution down to ~2nm. However, EBL process requires a long patterning time because nanostructures are patterned by an electron beam writing slowly. Also, high processing cost is required owing to the high cost equipment. This is the reason why electron beam lithography is not proper for mass production and various applications. Also, microfabrication is needed to fabricate the microchannel and reservoir in the nanochannel fabrication process. When two different scale fabrication is progressed gradually, hard alignment problem between nanopatterns and micropatterns is discussed. Complex bonding process is required to a fabricated sample due to the bonding with another cover slip.

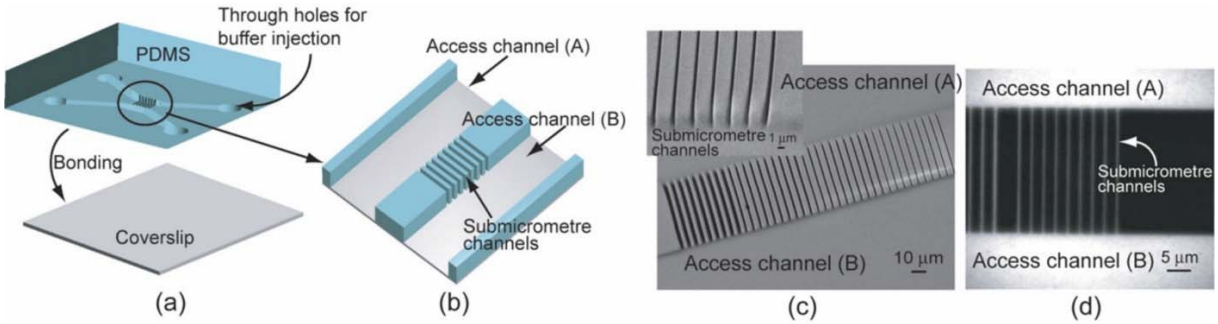

Figure 1.3 Images of the nanofluidic device fabricated by the electron beam lithography (EBL) from Yokokawa *et al.* [23]. Narrow and uniform pattern array was fabricated using EBL.

The focused ion beam (FIB) technology enables swelling, milling, implantation and ion-induced deposition [25]. FIB milling uses Ga+ ions without mask and photoresist for patterning the nanochannels. A principle of the FIB milling is similar to EBL and difference is the type of the beams. EBL uses an electron beam and FIB milling uses a focused ion beam. FIB also writes a designed pattern on the substrate using the focused ion beam. So, complex and elaborate patterns can be engraved to the substrate like the EBL. But, some limitation factors block wide utilization of FIB milling technique such as a costly equipment, low scanning speed and complex bonding process with another cover substrate. Figure 1.4 shows the schematic images of the FIB milling and SEM images of various size nanopatterns fabricated by the FIB milling. The pattern sizes were controlled by the thickness of a metal film and minimum pattern size is 5-nm.

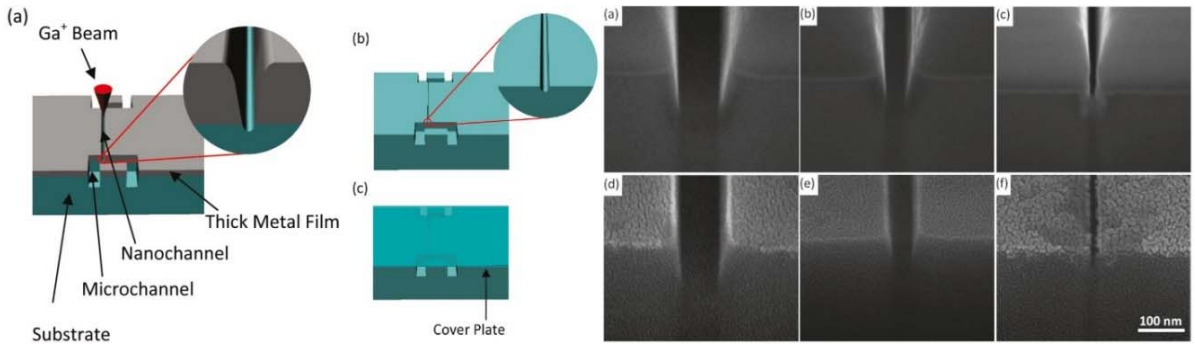

Figure 1.4 Images of the focused ion beam milling; Schematic images show the fabricated nanochannel with Ga^{+} beam and metal film, SEM images show the various dimensional nanochannels up to 5-nm from Menard *et al.* [24].

Figure 1.5 show the nano imprint lithography (NIL) fabrication process. NIL is a replication process using a mixed-scale hard master fabricated by the conventional micro-fabrication and nanofabrication. When a substrate coated with a curable resin such as a SU-8, PMMA is mechanically pressed by a master including the predefined micro-nanostructures using the

electron beam lithography or focused ion beam milling, the curable resin is cured by the UV light or heat in condition of controlled temperature and pressure. Finished replica is used to polymer molding process for a number of times. In this way, the master and replica can be used many times. Therefore, the NIL enables nanofluidic device to a massive production owing to the reproducible master and replica. Also, micro-nanopatterns can be transferred by a single fabrication process. However, there are mortal limitations of the NIL fabrication process. Expensive and complex nanolithography techniques such as EBL and FIB milling and etching process are also needed to fabricate the mixed-scale master. Also, the precise control of the pressure for large scale patterning, perfect removal of a residual layer and clean demolding after a mold treatment are challenges of the NIL. Besides, Inter ferometric lithography, sphere lithography and conventional MEMS technique such as a sacrificial layer releasing, etching and deposition can be applied to fabricate the nanochannel.

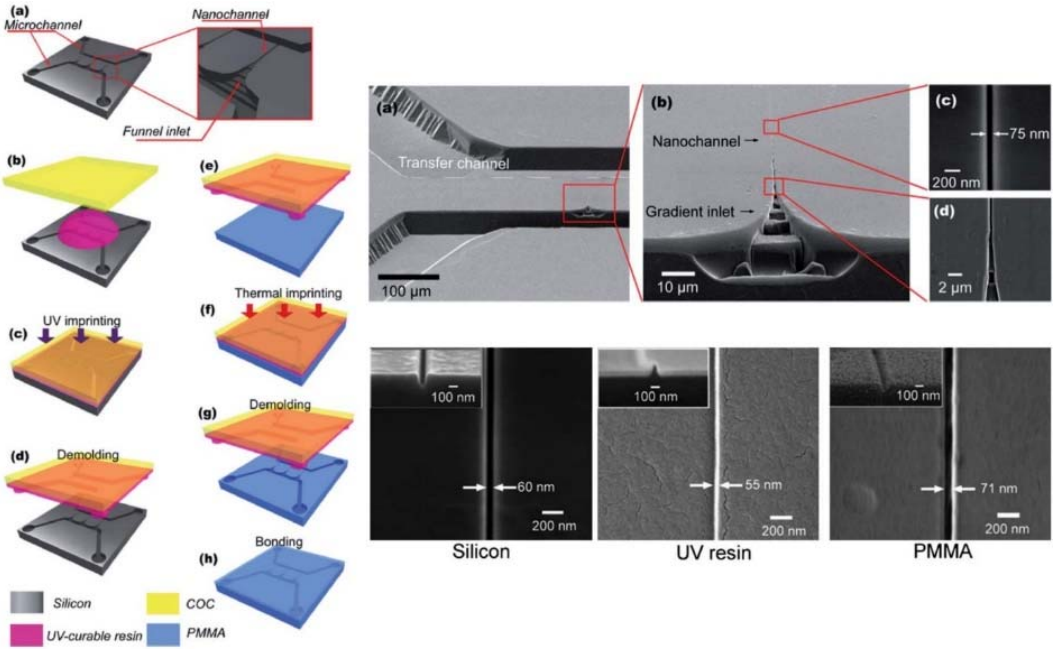

Figure. 1.5 3D fabrication flow and SEM images of the fabricated silicon, UV resin, PMMA structures from Chantiwas *et al.* [26]. Funnel and complex structures of the nanochannel inlet fabricated by FIB milling improve the efficiency of the DNA stretching.

1.2.2 Soft Material

Soft lithography using the polymers such as a Poly(dimethylsiloxane) (PDMS), Poly (methyl methacrylate) (PMMA), Poly (urethane acrylate) (PUA) have been widely used to research for the microfluidics, μ–contact printing, tactile sensor and NIL because of the easy process, low cost material, flexibility, transparency and biocompatibility [33]. Especially, fabrication based on the soft-polymer is a cost-effective and easy process in terms of the cost and their properties because soft-polymer can be replicated many times from the mold. Many research groups thought about the soft lithography as a powerful fabrication technique for the nanofluidic device. However, there are several problems such as a low modulus causing the distortion including pairing, sagging and shrinking. Some research groups have used this characteristics and developed a fabrication technique for an unconventional nanochannels [35-39]. Roof collapsed fabrication technique uses low modulus property of the PDMS. Chung *et al*. developed a fabrication technique for the roof collapsed triangular PDMS nanochannel using the microchannel [8, 34-36]. First of all, SU-8 micro structure with wide width was patterned by conventional UV lithography. Secondly, PDMS was molded and demolded from the microstructure. Finally, when PDMS microchannel bonded to the glass was roof collapsed, triangular nanochannels were formed at the side edge of the roof collapsed microchannel. Another research group has shown the result that roof collapsed PDMS channel arrays were stacked up each other and rolled up and then cut across the section to increase the channel arrays [37].

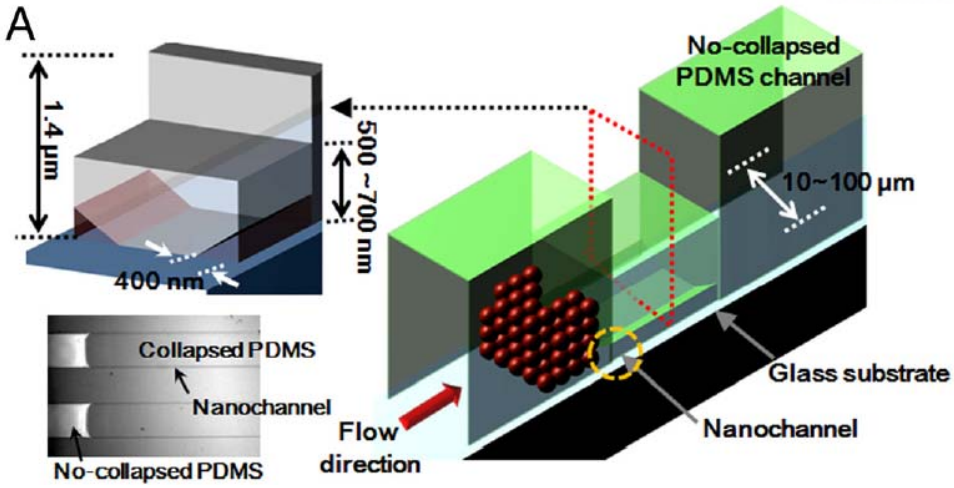

Figure 1.6 Schematic image of the roof collapsed nanochannels from Chung *et al.* [8]. Wide microchannel's roof was collapsed because of the low modulus of the PDMS and triangular nanochannels were formed at the edge of the collapsed microchannel.

Huh *et al.* has developed nanochannel array with Cracked PDMS in the microchannel [39]. Sylgard A and B was mixed by 10:1 weight ratio. After degassing process, PDMS was cured in the convection oven during 4 hours. Cured PDMS was treated by the oxygen plasma. After oxygen plasma treatment, nanoscale crack was formed on the oxidized PDMS surface by the mechanical stress. Cracked PDMS was molded and demolded by PUA to replicate the nanoscale cracks. Finally, Cured PUA was molded by the PDMS the same way with first step. Demolded PDMS from the PUA was bonded to glass substrate by the oxygen plasma treatment. Another researcher called this nanochannel to winkle nanochannel (WNCs) and applied for the protein preconcentration [7].

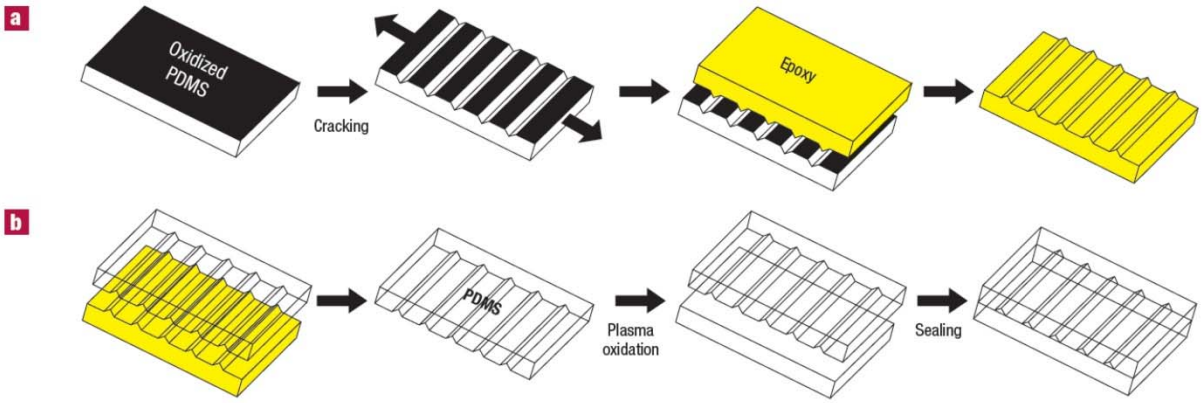

Figure. 1.7 Schematic images of the fabrication process of the cracked induced PDMS nanochannel arrays from Huh *et al.* [39]. Cracked nanochannels on the oxidized PDMS surface are replicated using epoxy.

Meanwhile, Schmid *et al.* developed the hard PDMS that has a remarkable property for soft lithography such as a high modulus than the soft PDMS [33]. Odom *et al.* compared hard PDMS to soft PDMS that is sylgard 184 and demonstrated in the paper [34]. Perry *et al.* developed the nanofluidic funnels using the hard PDMS to research the ion transport across the nanofluidic funnel [1]. Hard PDMS mixture including a vinyl PDMS prepolymer, a hydrosilane PDMS prepolymer, a platinum catalyst and a modulator was spin-coated on the silicon mold fabricated by the EBL. Soft PDMS (Sylgard 184 mixture) was poured on the thin hard PDMS layer and cured in the convection oven. Demolded PDMS including the hard PDMS and the soft PDMS layer was bonded to the glass substrate by the oxygen plasma treatment. In such ways, various soft materials is used to fabricate the nanochannels through an unconventional fabrication techniques.

1.3 Carbon MEMS

Carbon-MEMS (C-MEMS) is an innovative technique that can overcome many limitations of the microfabrication and nanofabrication techniques. There are plenty of the problems for example separately processed microfabrication, nanofabrication and hard alignment, time consuming process and high cost. In the C-MEMS process, a microstructure is made by the conventional microfabrication method such as a UV lithography and etching. The microstructure dimensions are reduced up to a sub-100-nm nanostructure after the pyrolysis process owing to enormous volume shrinkage [40-42]. So C-MEMS technique enables to fabricate the monolithic nanochannel master by the batch fabrication process without hard alignment problem between nanofabrication and microfabrication. Meanwhile, C-MEMS technique almost has been used for electrode material because of the wide electrochemical stability, biocompatibility, chemical inertness and low cost.

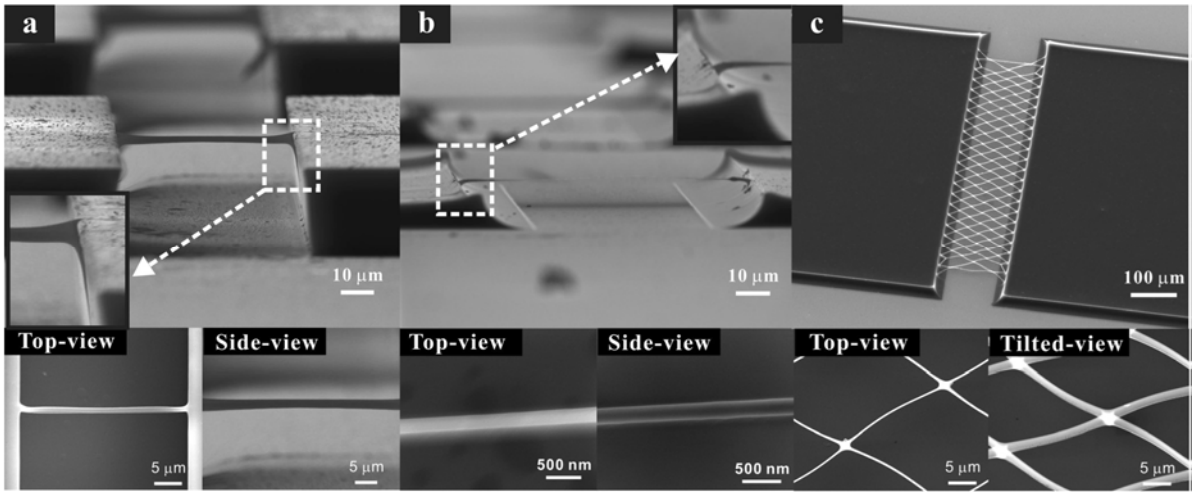

Figure 1.8 SEM images of the suspended single wire and meshes structures fabricated by the carbon MEMS from Lim *et al.* [41]. (a) SU-8 suspended wire, (b) After pyrolysis, suspended carbon nanowire, (c) suspended carbon nanomeshes structure. Enormous volume shrinkage occurred during the pyrolysis process is verified by this images.

Also, glassy carbon converted from a photoresist has a conductivity characteristics. In this research, enormous volume shrinkage characteristics of many advantages was focused to fabricate the monolithic mixed-scale carbon structure for the mixed-scale PDMS channel. A limitation that photolithography is only microfabrication owing to the UV light wavelength size can be overcame using the pyrolysis process. After pyrolysis, dimensions of the carbon structure is predictable because of the ratio of reduction. Polymer structure volume shrinks around 80 % at temperature above 400 °C. So, carbon structure dimension can be control by the type of the photoresist, a revolution per minute (RPM) of a spin-coating. In real situation, 1-μm-width and 300-nm-thickness polymer structure was converted to the nanoscale carbon structure including 441-nm-width and 55-nm-thickness. Also, carbon structure shape is freely controlled owing to the UV lithography. In the carbon- MEMS, All advantages of the UV lithography can be applied such as an easy alignment, shape and dimension control through the design of a photomask. Also, surface energy of the carbon is changed gradually depending on the pyrolysis temperature. Surface energy is remarkably increased between 400 °C to 500 °C because Solid carbon is formed at this temperature region. Meanwhile, surface energy is important with an inclined side wall for the soft lithography for the easy demolding process from the structure. Also, a side-wall of the carbon structure is a sloped structure reminding a trapezoid. This phenomenon is occurred because of the difference of the diffusion rate between the top of the structure to the sides of the structure. As a result, gradually tapered 3D-microfunnel and easily demolded inclined side wall structure can be fabricated during the carbon MEMS process. For these reason, C-MEMS technique was used mainly to fabricate the mixed-scale PDMS channel networks in this research.

1.4 Thesis Outline

In this thesis, the novel and innovative fabrication technology for the mixed-scale PDMS channel networks monolithically will be described by the C-MEMS technique and a PDMS molding process. Newly developed fabrication is largely made up 2-steps photolithography, pyrolysis and single molding process using the hard PDMS and the soft PDMS. Built-up mixed-scale carbon structure can be used to excellent channel mold because of the excellent demolding efficiency. Usually, a master structure for the soft lithography based on the SU-8 are treated by chemical as an anti-adhesion layer coating. On the other hand, carbon mold needs no anti-adhesion layer coating. Because a SU-8 structure is converted to the pyrolyzed carbon structure with a change of the surface energy during the pyrolysis process. The carbon structure shows that the carbon structure is reproducible at least 40 times demolding process. Surface characteristics of the carbon structure will be shown by X-ray Photoelectron Spectroscopy (XPS), Energy Dispersive X-ray spectroscopy (EDS) and surface energy calculated by the Owens-Wendt geometric mean equation [43] using the measured contact angles of the water and the diiodomethane. Uniformity and hermetic sealing of the mixed-scale PDMS channel networks was demonstrated by the fluorescein isothiocyanate (FITC) imaging. Nanofluidic property of the mixed-scale channel was characterized by a current measurement. Current across the nanochannel shows the three different current regions including ohmic, overlimiting and limiting current regions. Finally, the mixed-scale PDMS channel network drives as a mixed-scale fluidic device. Functionality of the mixed-scale channel device will be shown by the micro-particle trap reminding the nanoelectroporation dedicating the efficient transfection.

2

Fabrication

In this chapter, a mixed-scale PDMS channel networks will be designed and fabricated. Also, completed polymer and carbon structure, PDMS channel dimensions will be shown in this chapter by SEM images and AFM profiles.

2. Fabrication of mixed-scale PDMS channel networks

2.1 Overview of the fabrication process

2.1.1 Mixed-scale carbon mold

The mixed-scale PDMS channel network was fabricated through two step UV lithography, the pyrolysis and simple molding process using the PDMS. First of all, initial photomask including 24 sets mold patterns shown by Figure 2.1 (a) and final photomask including 36 sets mold patterns of the 3-D microfunnel shown by Figure 2.1 (b) were designed by the auto CAD software program for the UV lithography. The fabrication process flow is shown in Figure 2.1. Firstly, bare silicon wafer was cleaned with deionized (DI) water and is spin-coated by thin negative photoresist (SU-8 2000.5) to fabricate the nanoscale structure after the pyrolysis step. The substrate uniformly coated with thin photoresist was soft baked on the hot plate at 95 ^{o}C during 1min and completely cooled down at room temperature. Si wafer was post-exposure-baked on the hot plate at 95 ^{o}C during 1min after UV light was exposed with vacuum contact on the substrate. The cool substrate was developed using the SU-8 developer during 1 min. Developed thin polymer structure was inspected to check the completeness and cleanness. Second UV lithography is for a formation of the microscale structure. Thick negative photoresist (SU-8 2010) was spin-coated at 2000 rpm for 30 sec with low rotation process to spread the photoresist and soft baked at 95 ^{o}C during 6 min on the hot plate. Sufficiently cooled substrate was UV exposed with vacuum contact for 10 sec and then post baked at 95 ^{o}C during 6min on the hot plate. After cooling process, UV exposed photoresist was developed in the SU-8 developer. The wafer including the final mixed-scale SU-8 structures was placed in the tube furnace with a high vacuum condition. The temperature of the tube furnace increases up to 900 ^{o}C for the pyrolysis and

the argon gas was used as non-oxidation gas. After the pyrolysis process, microscale SU-8 structure was successfully converted to the mixed-scale carbon structure.

2.1.2 PDMS channel network

Soft PDMS and hard PDMS were used for the simple soft molding process to fabricate the mixed-scale PDMS channel networks. A vinyl PDMS prepolymer, a hydrosilane PDMS prepolymer, a platinum catalyst and a modulator were mixed respectively at the rate of 3.4 g, 1.0 g, 18 μL and 4 μL. Hard PDMS mixture was thoroughly added and located in the vacuum vessel to remove the bubbles. Hard PDMS mixture was properly poured and spin-coated at 1000 rpm for 40 sec to form the hard PDMS thin layer. The substrate coated with hard PDMS was cured at 60 ºC during 30 min in the convection oven. Soft PDMS is mixed with sylgard184 A (base) and B (curing agent) at a weight ratio of 10:1 and degassed in a small vacuum vessel to eliminate the bubble in the PDMS. Degassed soft PDMS was poured on the hard PDMS coated-substrate without anti-adhesion layer deposition and located at the room temperature for 10min to percolate down throughout a total area. Soft PDMS was cured at 65 ºC for 4 hours in the convection oven. After cooling time, soft PDMS and hard PDMS was peeled off from the substrate. The reservoir was holed by the biopsy punch to insert the fluid into the channel. The mixed-scale PDMS channel was bonded to the cover glass using the oxygen plasma treatment.

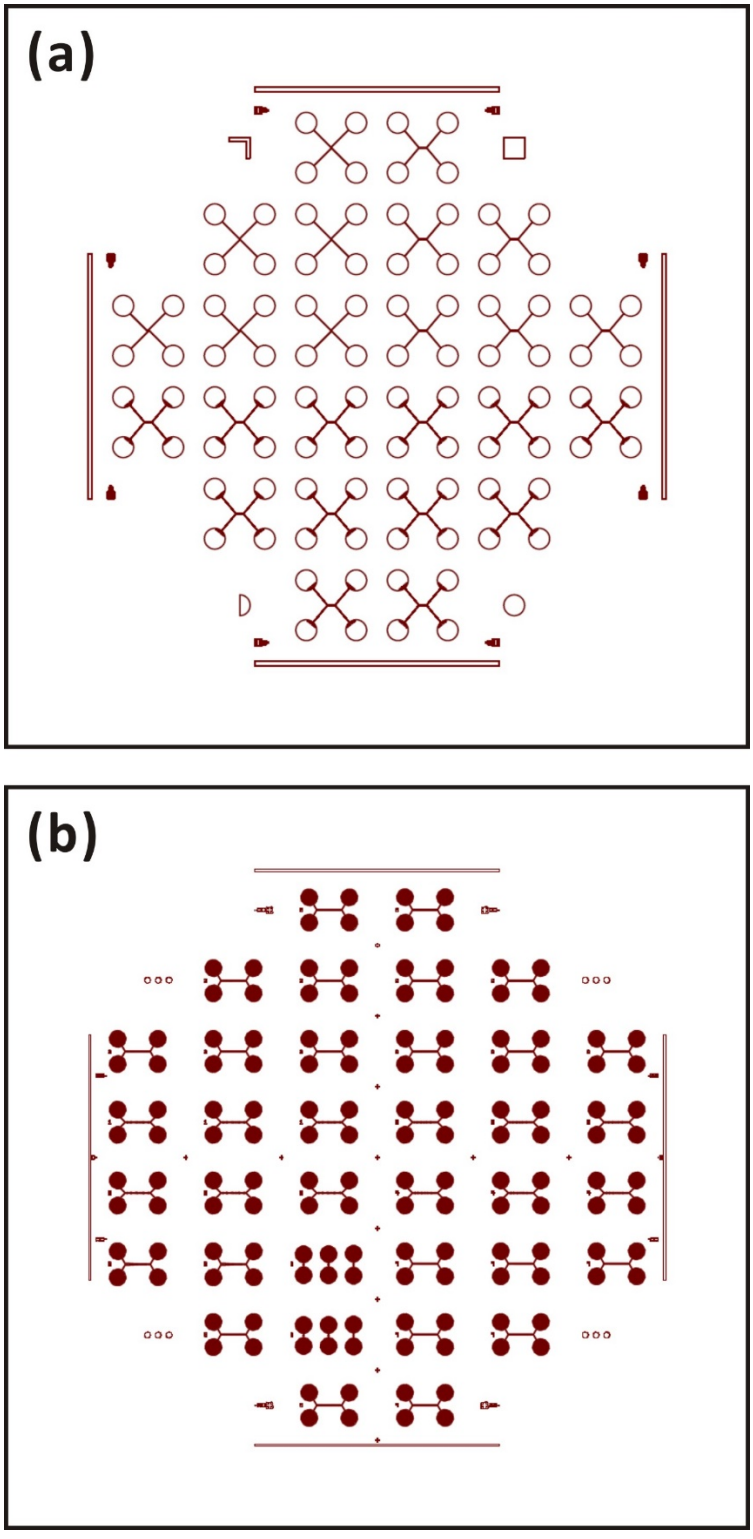

Figure 2.1 Designed photomask patterns for the mixed-scale PDMS channel networks by the auto CAD software. (a) Initially designed photomask including 24 sets of channel patterns, (b) Final photomask including 36 sets channel patterns with 3-D microfunnel.

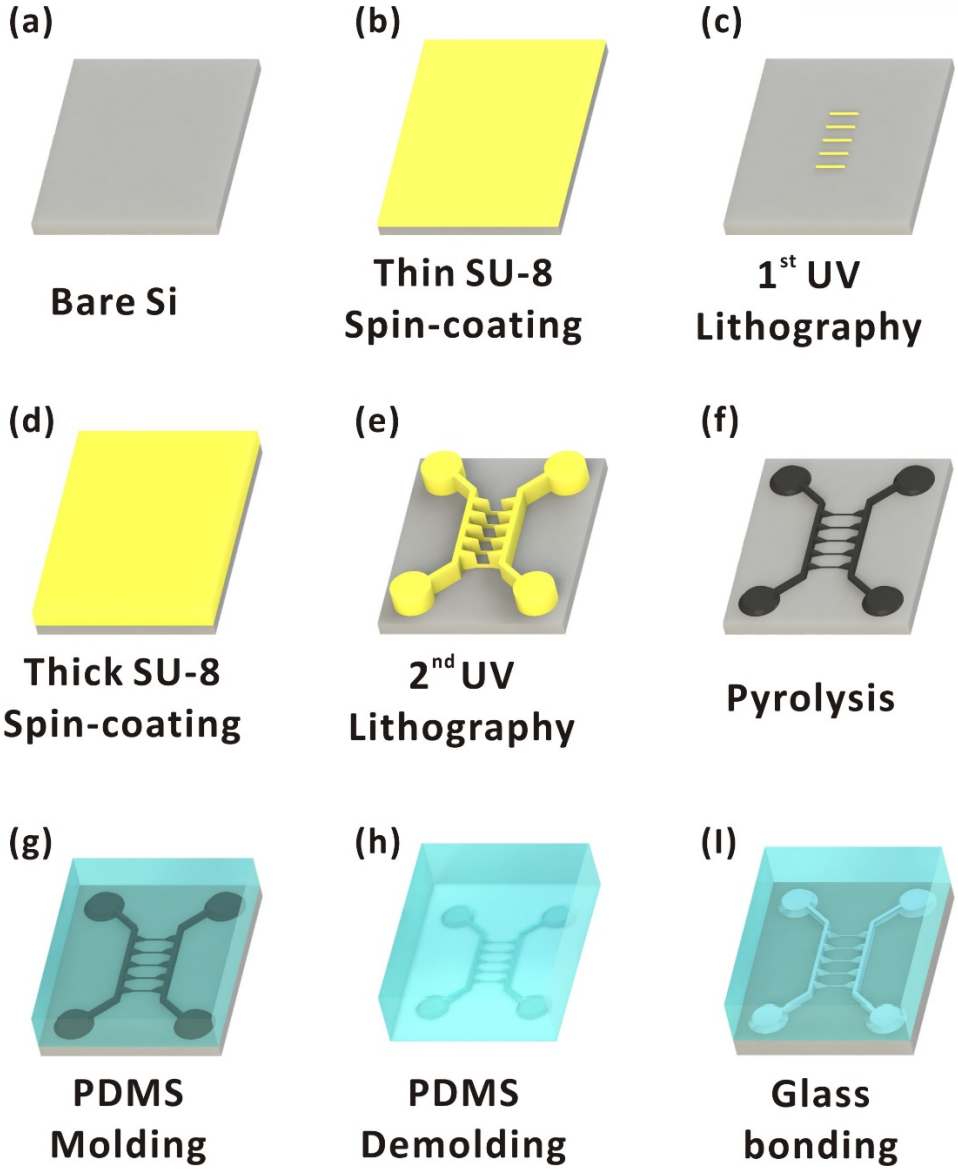

Figure 2.2 Schematic fabrication steps for PDMS mixed-scale channel networks. (a-e) 2-step UV lithography for fabricating mixed-scale negative photoresist (SU-8 2000.5 and SU-8 2010) structure. (f) Pyrolysis: the polymer structure is converted to the mixed-scale carbon structure with enormous volume shrinkage. (g-h) Soft molding: the mixed-scale carbon structures are replicated by a multilayered PDMS plate (hard PDMS and soft PDMS). (i) Glass bonding: the PDMS plate is bonded to the glass using oxygen plasma treatments.

2.2 Results

Successfully fabricated SU-8, carbon structures and PDMS channel are shown in Figure 2. 3. This structure was fabricated using the initial photomask patterns. Micro-holes in the SU-8 structure and carbon structure became the micro-pillar structures preventing the roof collapse of the PDMS. SU-8 structure with micro-holes was pyrolyzed to the volume shrunk mixed-scale carbon structure and carbon structures were transferred into the PDMS by the PDMS molding process. SEM images demonstrate that SU-8 structure was converted to the mixed-scale carbon structure without change of the original shape and the mixed-scale carbon structure was transferred to the precisely patterned PDMS channel without the changes of the original shape and size.

Table 1. The dimensions of the nanostructure of SU-8, pyrolyzed carbon and PDMS.

Material / Dimension	SU-8	Carbon	PDMS
Thickness	330 nm	55 nm	55 nm
Width	1.1 μm	441 nm	441 nm
Length	100 μm	121 μm	121 μm

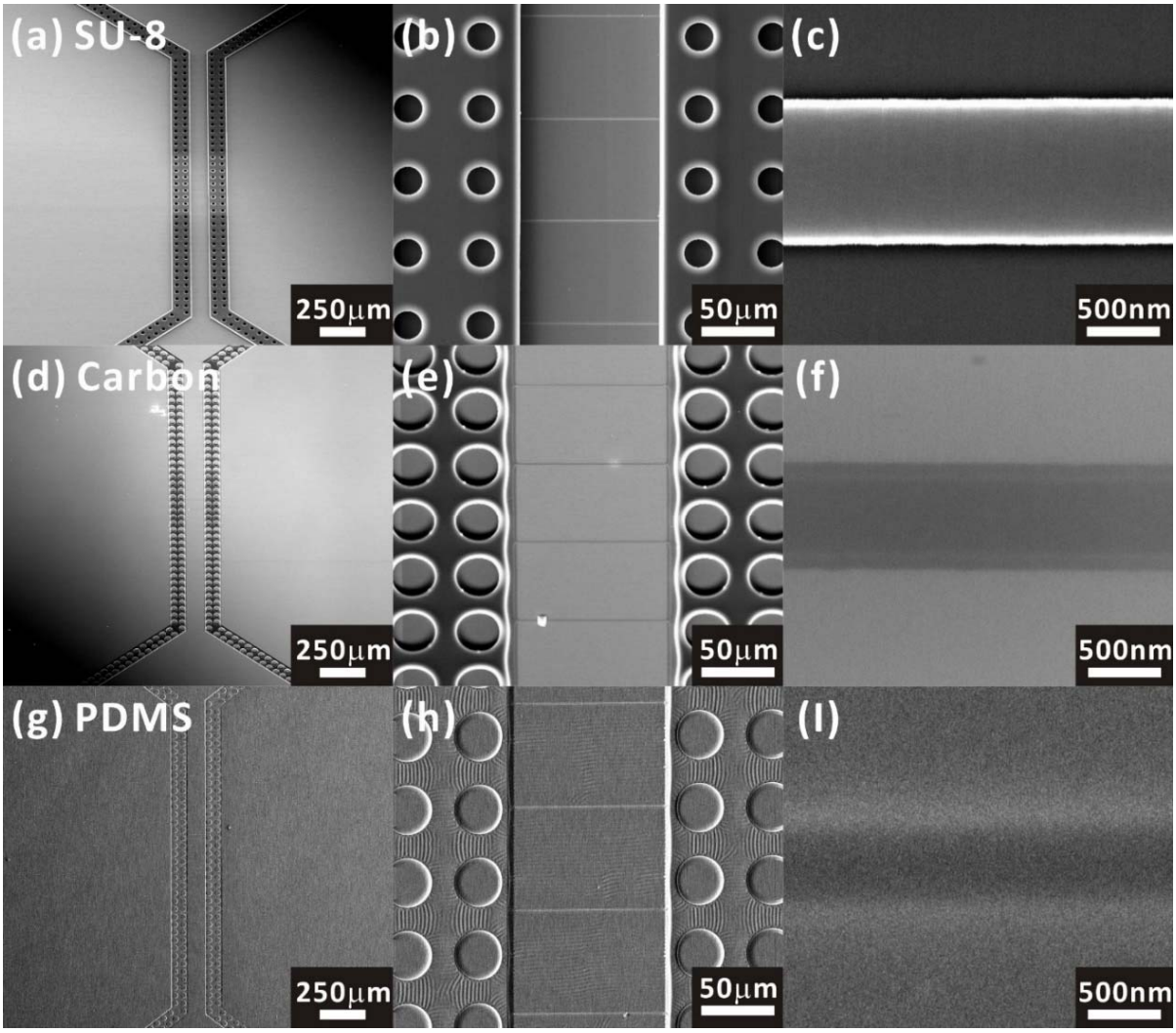

Figure 2.3 SEM images of (a-c) a SU-8 photoresist structure with micro-holes, (d-f) a pyrolyzed carbon structure with micro-holes and, (g-i) a demolded PDMS structure with micro-pillars from the pyrolyzed carbon structure (d-f). Micro-holes in the SU-8 and carbon structures were transferred into the micro-pillar structures preventing the PDMS roof collapse in the PDMS.

Figure 2.4 shows the side walls of the SU-8 photoresist structure and carbon structure after pyrolysis process. Vertical side wall of the SU-8 photoresist was converted to the gradually inclined-side-wall. This phenomenon occurs only after pyrolysis process because the different diffusion rate between a top and a side during the pyrolysis process. This structure is expected to help easy demolding process of the PDMS from the carbon structure. Also, the PDMS channel demolded from this carbon structure with inclined side wall can be applied to the efficient particle trap using the unique sidewall shape.

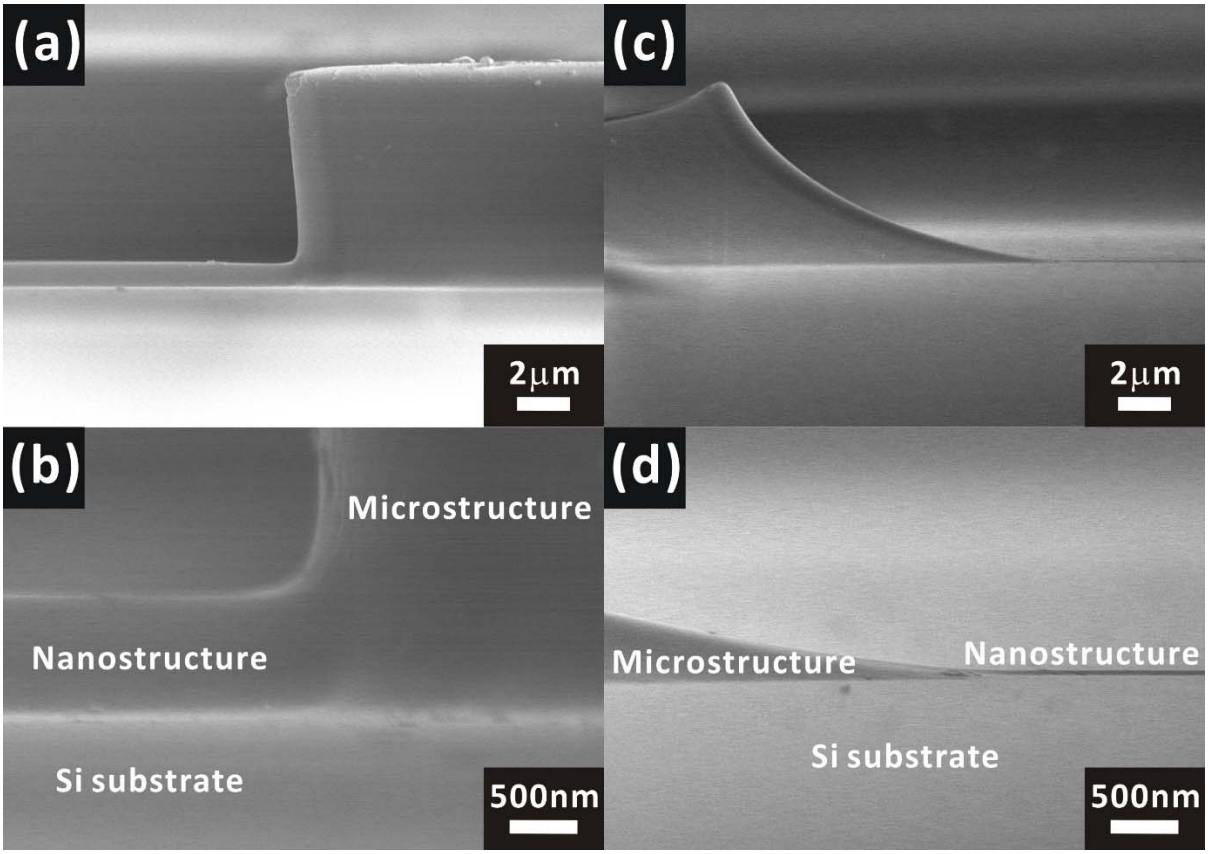

Figure 2.4 SEM images of the side walls; (a-b) the SU-8 structures after 2-steps UV lithography, (c-d) the mixed-scale carbon structures with gradually inclined side wall after pyrolysis.

Figure 2.5 is 3-D profiles showing the uniformly arrayed topographies of the SU-8 mold, pyrolyzed carbon mold and PDMS channel measured by the atomic force microscopy (AFM). This images show that SU-8 structure including a wide and high dimension is converted to low dimension carbon structure. After PDMS demolding process, prominent carbon structure is transferred into the PDMS precisely.

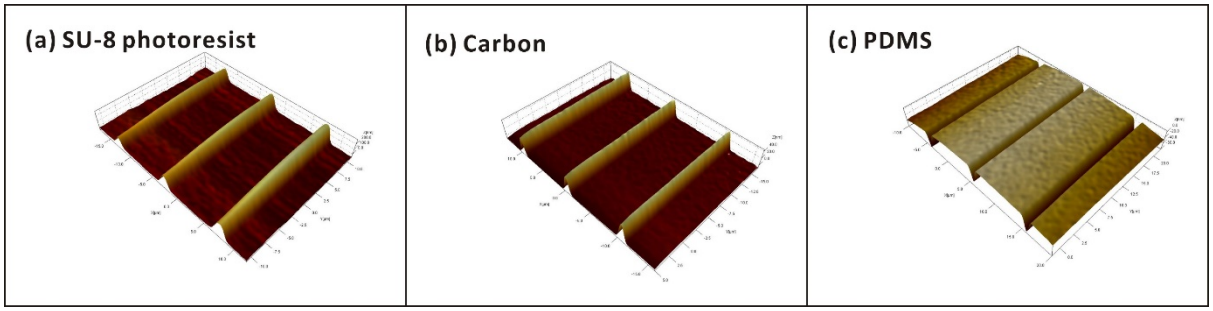

Figure 2.5 3-D AFM images of (a) SU-8 structures before pyrolysis, (b) carbon molds for nanochannels, and (c) PDMS nanochannels.

SEM images of the completed SU-8 photoresist structure and pyrolyzed carbon structure including the 3-D microfunnels are observed in Figure 2.6. (a)-(d) are SEM images of the 60^{o} microfunnels including the 60^{o} inlet angles. (a) and (b) are respectively top view and tilted view of the SU-8 photoresist structures. (c) and (d) are top view and tilted view of the pyrolyzed carbon structures. Thus, (e)-(h) are SEM images of the wide microfunnels including wide inlet angles greater than 60^{o}. (e) and (f) are respectively top view and tilted view of the SU-8 photoresist structures. (g) and (h) are top view and tilted view of the pyrolyzed carbon structures. After pyrolysis process, the mixed-scale carbon structures shown by (c), (d), (g) and (f) are monolithically connected between microstructures and nanostructures although the around 1-μm miss alignment during the UV lithography.

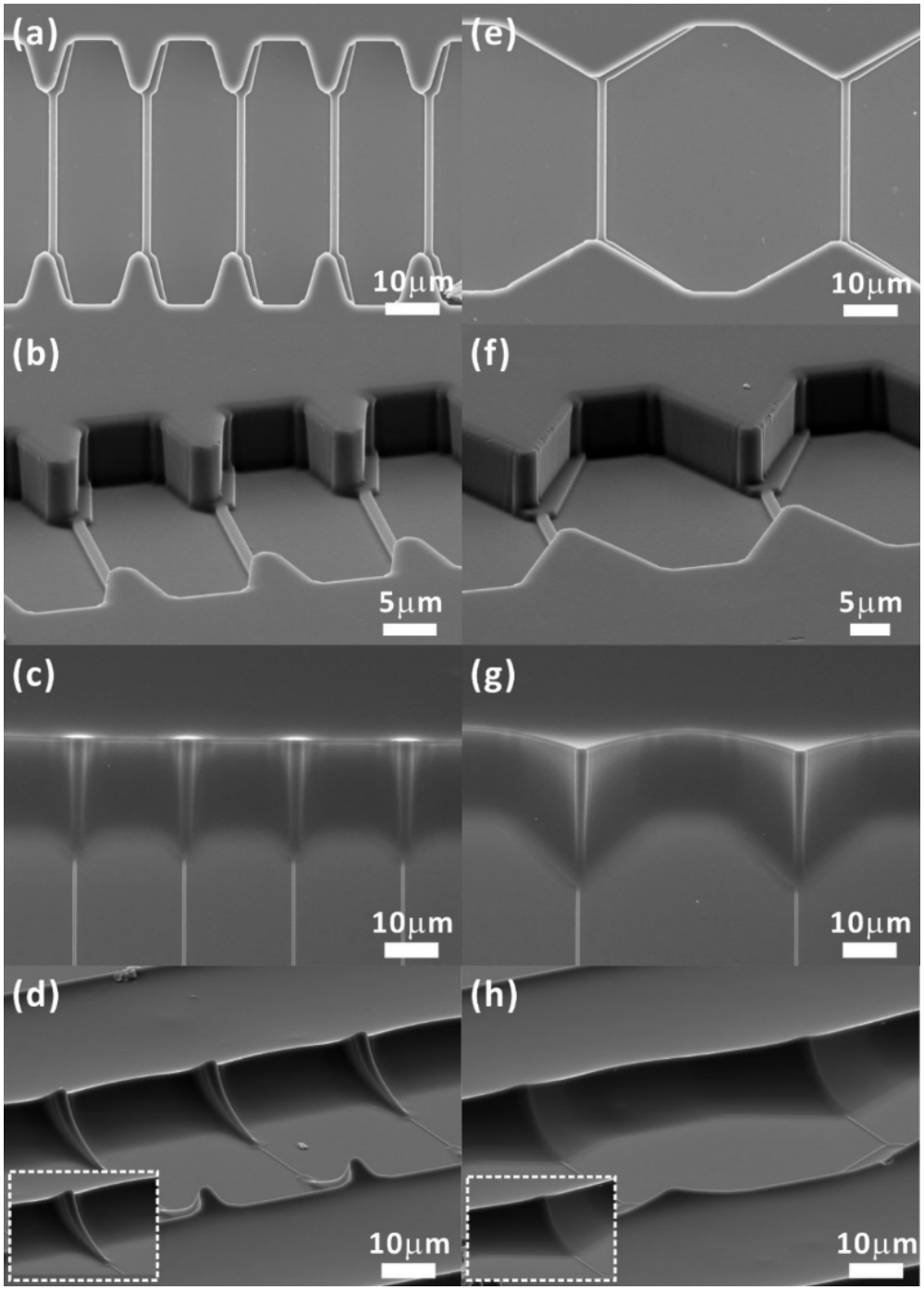

Figure 2.6 SEM images of the SU-8 structures and carbon structures. (a-d) Narrow 3-D microfunnel structures with inlet angle less than 60°: (a, b) the SU-8 structures, (c, d) the carbon structures corresponding to (a) and (b). (e-h) Wide 3-D funnel structures with inlet angle greater than 60°: (e, f) the SU-8 structures, (g, h) the carbon structures corresponding to (e) and (f).

Meanwhile, various carbon structures are shown in Figure 2.7. Letters, geometric structures and smoothly integrated mixed-scale structure can be fabricated by the carbon MEMS process. Because the photomask designs using the auto CAD enables the UV lithography to various shape patterning.

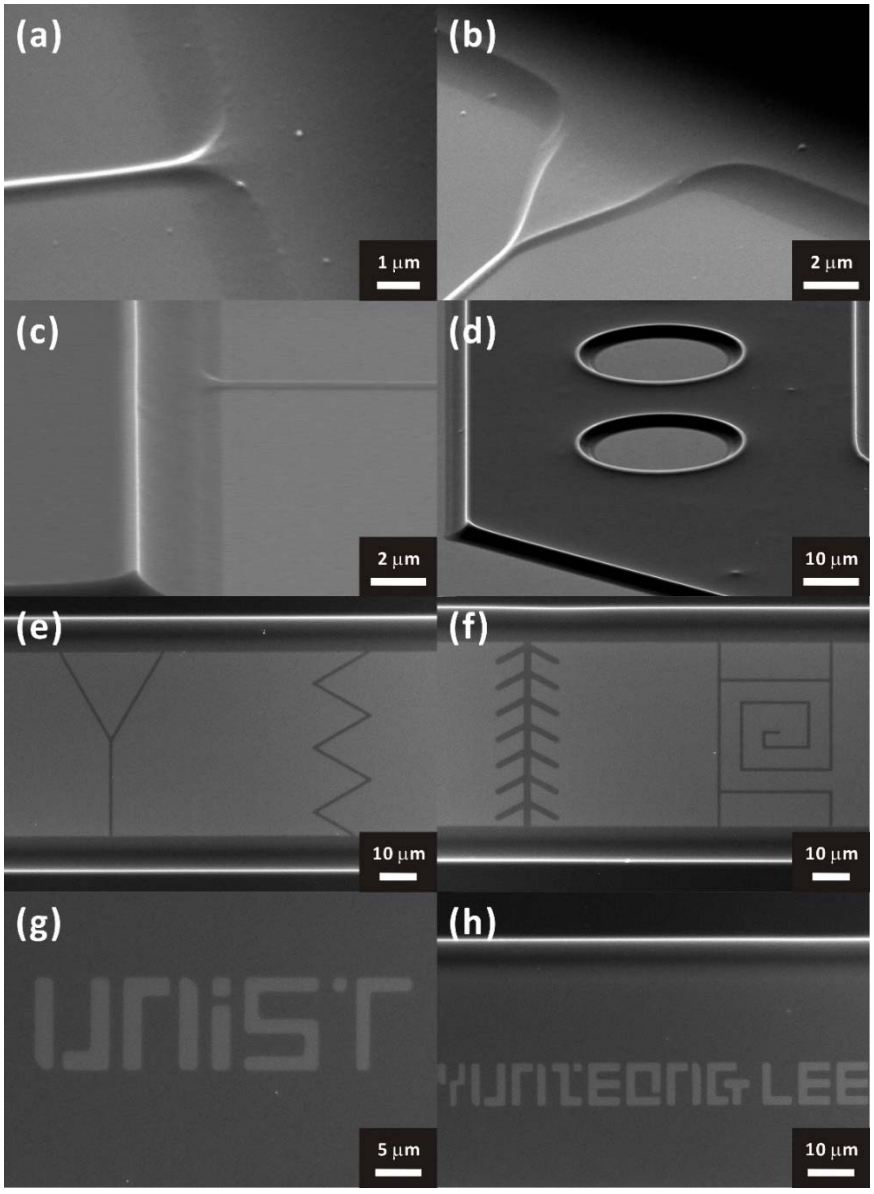

Figure 2.7 SEM images of the various shape pyrolyzed carbon structures; (a-b) nanofunnel structures, (c) Inclined side wall with nanostructure, (d) Microstructure with the microholes, (e-f) Geometric carbon structures, (g-h) Letters of UNIST and Yunjeong Lee.

3

Surface Characterization

Surface characterization was conducted by the surface free energy by the contact angle measurement, demolding test using the PDMS and analysis by the XPS and EDX.

3. Characterization of pyrolyzed carbon surface

Surface characteristics of the pyrolyzed carbon was measured by the contact angle measurement, the calculation of the surface free energy using Owens-Wendt geometric mean equation, demolding test and surface analysis using XPS, EDS. Surface free energy is the attractive energy that pulls an external materials by the attraction of the shell atoms. Hydrophobicity and hydrophilicity of the surface are determined by surface free energy. In other word, a hydrophobic surface has a low surface energy and a hydrophilic surface has a high surface energy. These two properties of the surface are important and have merits and demerits. For example, hydrophobicity of a surface holds the limelight as an anti-fouling technique including 'the lotus effect'. In soft lithography, hydrophilic surface including a high surface energy is needed to transfer the patterns into the PDMS by high adhesion for the μ-contact printing (μCP) [43]. In the surface for a channel mold, hydrophobic surface including a low surface free energy is better than hydrophilic surface for a clear and easy demolding process owing to low adhesion strength [44]. Therefore, the surface including the high surface energy is modified to low the surface free energy by the anti-adhesion layer coating. However, anti-adhesion layer coating has some problems such as a lack of uniformity of the anti-adhesion layer deposited by vapor phase evaporation, toxicity of the solution and spending too much time for deposition of the anti-adhesion layer [44]. In this thesis, surface free energy was calculated by Owens-Wendt geometric mean equation based on the contact angle on the carbon surface. Also, demolding efficiency of the carbon mold was tested by the PDMS demolding repetition test. Demolded carbon samples and bare carbon sample are analyzed by contact angle, XPS and EDS.

3.1 Contact angle measurement

SU-8, pyrolyzed carbons at various temperatures from 300 ºC to 900 ºC and the anti-adhesion layers coated 900 ºC carbon samples were prepared to measure their contact angles. Carbon sample pyrolyzed at 900 ºC was placed in vacuum chamber and the chrolotrimethylsilane (Silane) was evaporated during overnight for the vapor phase evaporation. After oxygen plasma treatment, another carbon sample was placed in the 2% (3-Aminopropyl) triethoxysilane (APTES) solution with the ethanol at the room temperature during 2 hours for the liquid phase deposition. After the carbon sample coated by APTES was placed in the convection oven during 30 min, the sample was rinsed by ethanol and dried. Contact angle was measured more than 8 times using other samples by the deionized water (H_2O) and the diiodomethane (CH_2I_2). All samples were used only one time because the wetting contact angle of one time wetted surface is always smaller than the first contact angle. Measured contact angles of the all samples were calculated and analyzed by Owens-Wendt geometric mean equation [45].

3.2 Surface free energy calculation by Owens-Wendt geometric mean equation

Owens and Wendt defined to the equation for the surface free energy using the two components in 1969. Owens-Wendt equation starts from Young's equation. This equation is popular because the polar interaction and the dispersive interaction on the solid surface are considered. The dispersive component and polar component are considered by van der Waals interaction and polar forces including the Debye interaction and hydrogen bond interaction. So, two liquids consisted of dispersive and polar components are required to define the surface free energy using the Owens-Wendt equation. Water and diiodomethane are well known as polar and dispersive component liquids respectively. The Owens-Wendt geometric mean equation is as in the following.

$$\gamma_{LV}(1+\cos\theta) = 2\sqrt{(\gamma_S^D \gamma_L^D)} + 2\sqrt{(\gamma_S^P \gamma_L^P)}$$

$$\gamma_S = \gamma_S^D + \gamma_S^P$$

In this equation, abbreviated L, S, D, P mean liquid, solid and dispersive and polar components. γ_{LV}, γ_L^D and γ_L^P are the reported values as the surface tension of the liquids. The γ_L^D and γ_L^P of the water are 22.85 dyne/cm and 50.3 dyne/cm. Also, the γ_L^D and γ_L^P of the diiodomethane are 48.5 dyne/cm and 2.3 dyne/cm. θ is measured contact angle. Finally, the surface free energy γ_s is the sum of the polar surface energy γ_S^P and the dispersive surface energy γ_L^D.

3.3 Demolding efficiency

Carbon mold efficiency was measured by continuous PDMS molding and demolding experiment of the same carbon mold. Three different carbon surface samples including the vapor phase evaporation by Silane, liquid phase deposition by APTES and unmodified carbon surface were prepared. PDMS mixture was poured respectively on the carbon mold surfaces and degassed in the vacuum chamber. The degassed PDMS was cured during 4 hours at 65 ^{o}C in the convection oven. After sufficient cooling time, PDMS samples were peeled-off from the different carbon surfaces. Then, optical inspection using the optical microscope to check the overall changes, contact angle measurement on the demolded carbon and demolded PDMS and surface characterization using the XPS and EDS were performed immediately.

3.4 Results

The contact angles using the diiodomethane are approximately larger than the contact angles measured by the deionized water in the contact angle measurement. Figure 3.1 and Figure 3.2 show the results of the contact angle measurement with the optical microscopic images and graphs. Owens-Wendt geometric mean equation was applied for the analysis of the contact angle datas. Diiodomethane and deionized water present respectively dispersive component and polar component.

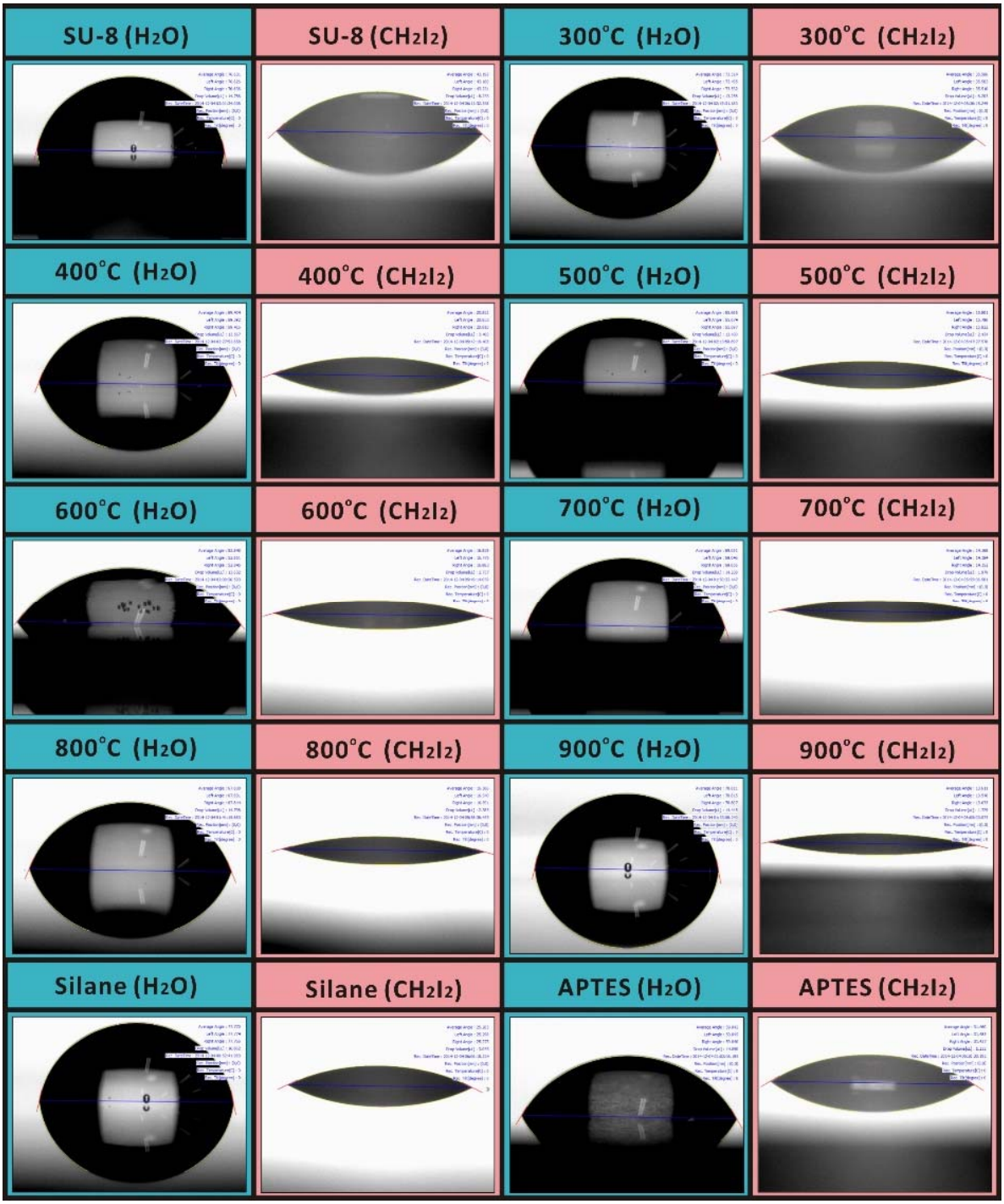

Figure 3.1 Images of the measured contact angles on the SU-8, pyrolyzed carbon at different temperatures from 300 ºC to 900 ºC and anti-adhesion-layer coated carbon surface using the deionized water and the diiodomethane for analysis of the surface free energy using the Owens-Wendt method. (All samples were measured at least 8 times.)

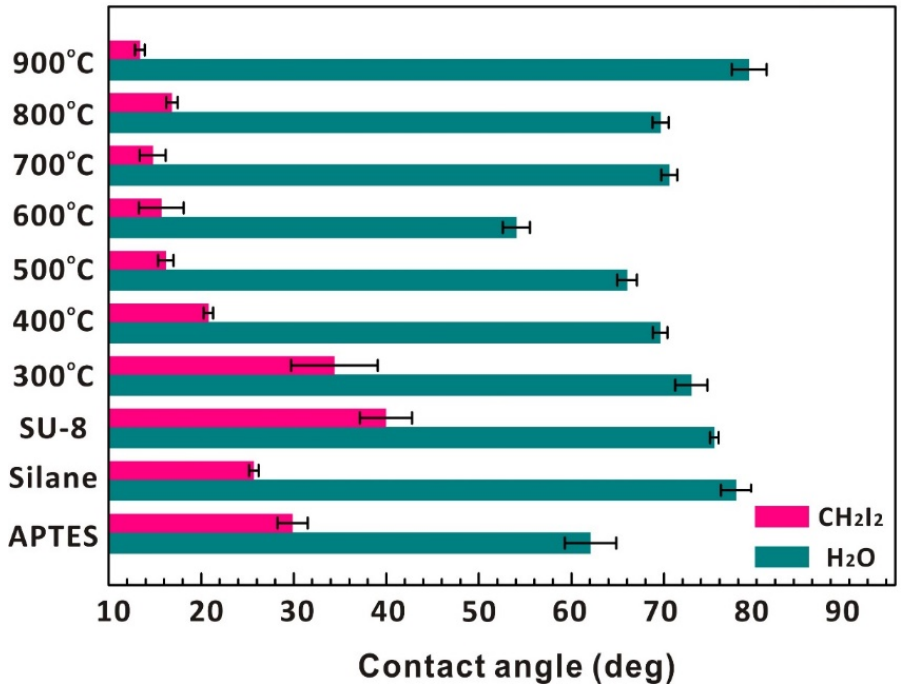

Figure 3.2 Contact angles graph on the on the SU-8, pyrolyzed carbon at temperature from 300 ºC to 900 ºC and anti-adhesion-layer coated carbon surface. Pink color bars were measured by diiodomethane and green color bars were measured by deionized water.

Table 2. Surface free energies of carbon samples pyrolyzed at various pyrolysis temperature from 300 to 900 ºC, and surface free energies of carbon samples (pyrolyzed at 900 ºC) coated with an anti-adhesion-layer using vapor-phase evaporation and the liquid-phase deposition.

Materials	Surface free energy [dyne/cm^2]
SU-8	40.89
Pyrolyzed carbon at 300 ºC	43.66
Pyrolyzed carbon at 400 ºC	48.75
Pyrolyzed carbon at 500 ºC	50.65
Pyrolyzed carbon at 600 ºC	54.98
Pyrolyzed carbon at 700 ºC	49.90
Pyrolyzed carbon at 800 ºC	49.66
Pyrolyzed carbon at 900 ºC	49.43
Silane (Vapor)	46.04
APTES (Liquid)	48.63

Surface free energies were calculated using the Owens-Wendt geometric mean equation. Table 2 shows the calculated surface free energies. Surface free energy increases as the increase of the pyrolysis temperature. Pyrolyzed carbon at 900 ºC is valuable. Because surface free energy is smaller than 700 ºC and 800 ºC. After 700 ºC, a dimension of the pyrolyzed carbon structure is minimum dimension after pyrolysis process. So, when the dimension of the pyrolyzed carbon is minimum, the smallest surface free energy is the pyrolyzed carbon at 900 ºC. So, the pyrolyzed carbon at 900 ºC was used for this research. Figure 3.3 is the graph of the demolding times before the break from the three different surfaces demolded including the unmodified carbon, coated carbon by Silane and by APTES. Firstly, the carbon structure coated with Silane using the chrolotrimethylsilane was destroyed after 3 times demolding process. Unmodified carbon structure and the coated carbon structure by APTES were broken respectively at 43 times and 50 times in order.

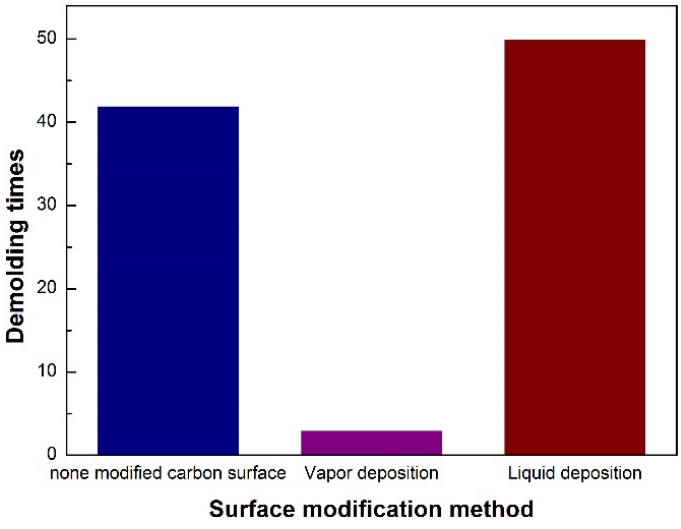

Figure 3.3 Graph of the comparison of the demolding times until damaged of the carbon mold using the three different carbon surface. Each samples were destroyed by 4 times demolding (vapor evaporation coated surface, purple), 43 times demolding (none modified surface, navy) and 50 times demolding process (liquid deposition coated surface, red).

Then, some experiments were performed to characterize each carbon surfaces. The contact angles were measured on the demolded three carbon surfaces and 1 time demolded PDMS surfaces from each carbon structure. Figure 3.4 shows the increase of the contact angle on the each surfaces after 1 time demolding process.

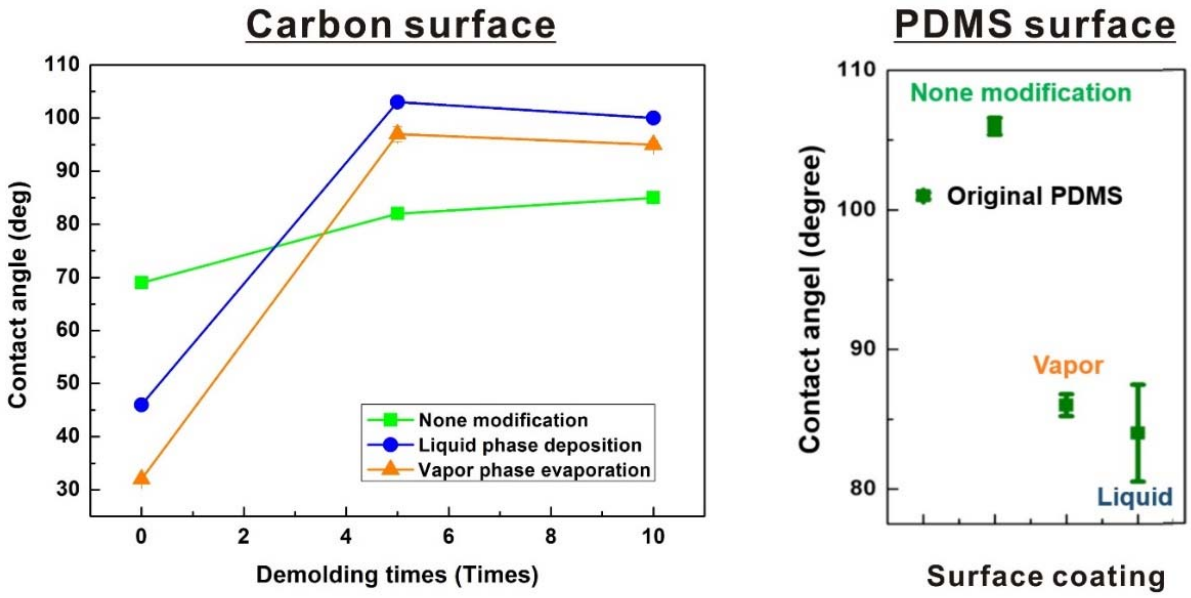

Figure 3.4 Graphs of the contact angle variation with demolding processes using the bare carbon sample, the anti-adhesion-layer coated carbon samples by vapor-phase evaporation and liquid-phase deposition; (a) contact angles of the carbon samples increase during the demolding process until 5 times, (b) contact angle of the 1 time demolded PDMS surface of three different carbon surfaces.

Also, XPS and EDS datas demonstrated that the coated Silane and APTES on the carbon surface as anti-adhesion layer were delaminated from the surface at 1 time demolding process because of the contact angle increase similar to PDMS and surface atomic ratio of main atoms changes. After demolding process, atomic ratio of the Si atom of the coated surfaces increased. This result shows that PDMS thin layer remained on the coated carbon surfaces

after demolding process. Through this characterization of the unmodified carbon surface and anti-adhesion layer coated carbon surfaces, several important phenomena were discovered. Firstly, the surface free energy of the carbon surface was changed as the chage of the pyrolysis temperature. Secondly, PDMS demolding times are different from the UV lithography condition and pyrolysis condition. Normally more than 40 times at least 4 times can be used to replicate the carbon structure using the PDMS regardless of the anti-adhesion layer coating in demolding experiment. Finally, anti-adhesion layer coatings using the vapor phase evaporation and liquid phase deposition are less effective than unmodified carbon surface because of unclear demolding of the PDMS. Therefore, the pyrolyzed carbon structures can be used to mold of the mixed-scale PDMS channel networks without anti-adhesion layer coating process.

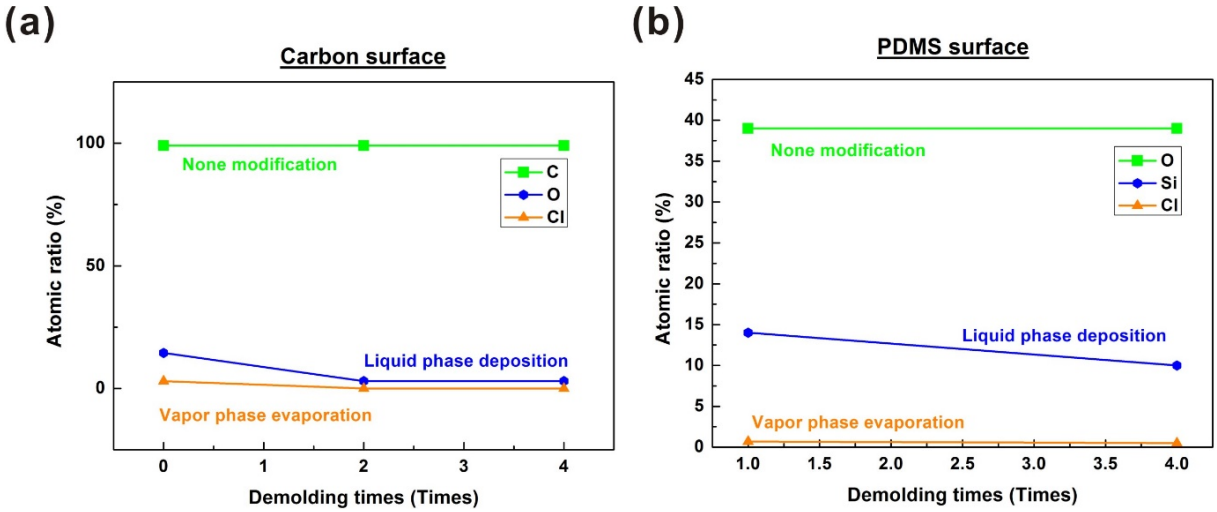

Figure 3.5 Energy dispersive X-ray spectroscopy (EDS) graphs of the demolded carbon samples and PDMS samples demolded from the carbon. (a) In the process of repeating demolding, atomic ratio of Chloride and Oxygen was gradually decreased on the coated carbon surfaces. (b) After 4 times demolding, atomic ratio of the silicon of the liquid-phase coated carbon and chloride of the vapor-phase coated carbon surface also decreases.

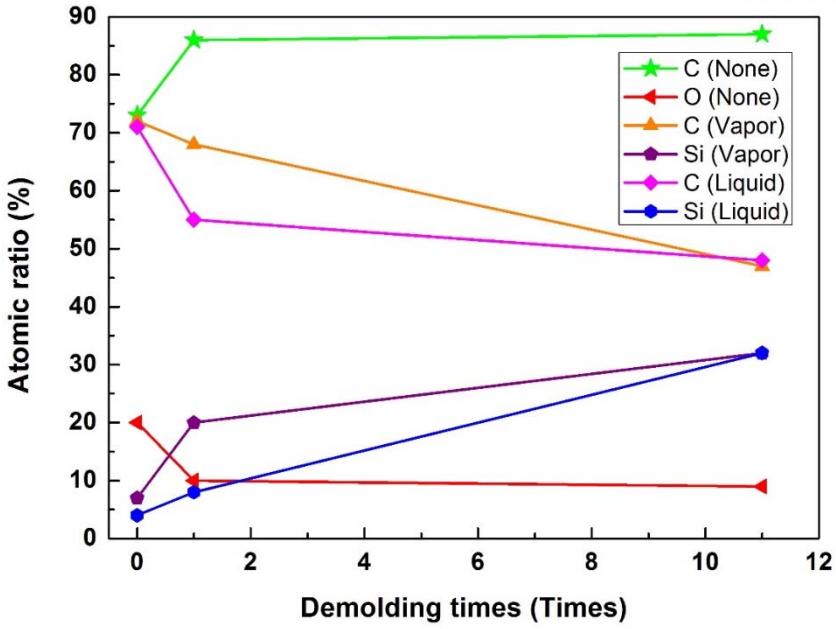

Figure 3.6 X-ray photoelectron spectroscopy (XPS) graph on three different carbon surfaces; None, vapor, liquid in graph mean none modified carbon surface, vapor phase coated carbon surface and Liquid phase coated carbon surface respectively. After 1 time demolding process, atomic ratio of all samples undergoes a sudden change.

4

Functionality test

In this chapter, functionality of the mixed-scale PDMS channel networks was tested by the Fluorescence image, current measurements and micro-particle trap in the 3D micro-funnel.

4. Functionality test of mixed-scale PDMS channel networks

The functionality of the mixed-scale PDMS channel networks was tested by the Fluorescence analysis using the fluorescent material, Current measurement and micro particle trap test in the 3D-microfunnel. Confocal microscope was employed for fluorescence analysis for hermetic channel sealing and nanochannel uniformity. The property of the nanofluidics was confirmed by formation of the three different current regions including the ohmic current, limiting current and overlimiting current. Finally, micro particles were trapped in the 3D microfunnels

4.1 Test for hermetic sealing

Fluorescein analysis was performed to confirm the uniformity and functionality of the mixed-scale channel without a solution leakage and a channel transform. A 0.1mM fluorescein isothiocyanate (FITC) solution was prepared in the DI water. The solution was filled in the mixed-scale PDMS channel networks including the nanochannel and microchannel from the reservoirs by the capillary force. The inverted microscope was utilized to observe and analyze the fluorescence in the mixed-scale PDMS channel networks. Figure 4.1 is the fluorescence image of the nanochannel arrays filled uniformly without solution leakage. Also, (a), (b) in Figure 4.1 show the coincident arrays between fluorescence image and SEM image. Figure 4.2 shows the 3-D intensity image scanned by height directions of the microfunnels filled with 0.1mM FITC solution. This image shows the gradually tapered 3D-microfunnel structure roughly.

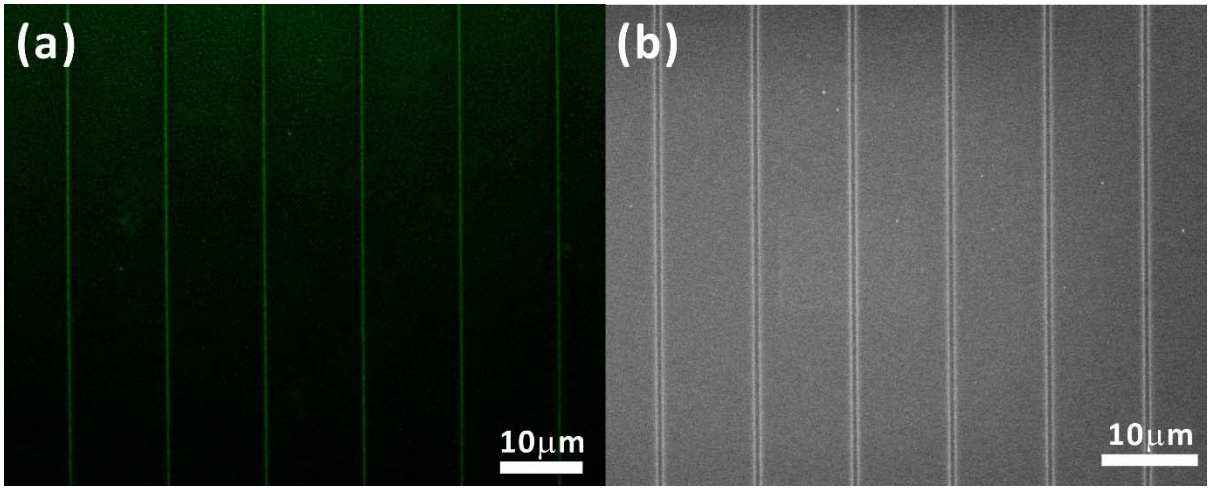

Figure 4.1 (a) Fluorescence microscopy image of a PDMS nanochannel array filled with 1 mM FITC solution; (b) SEM image of the PDMS nanochannel array.

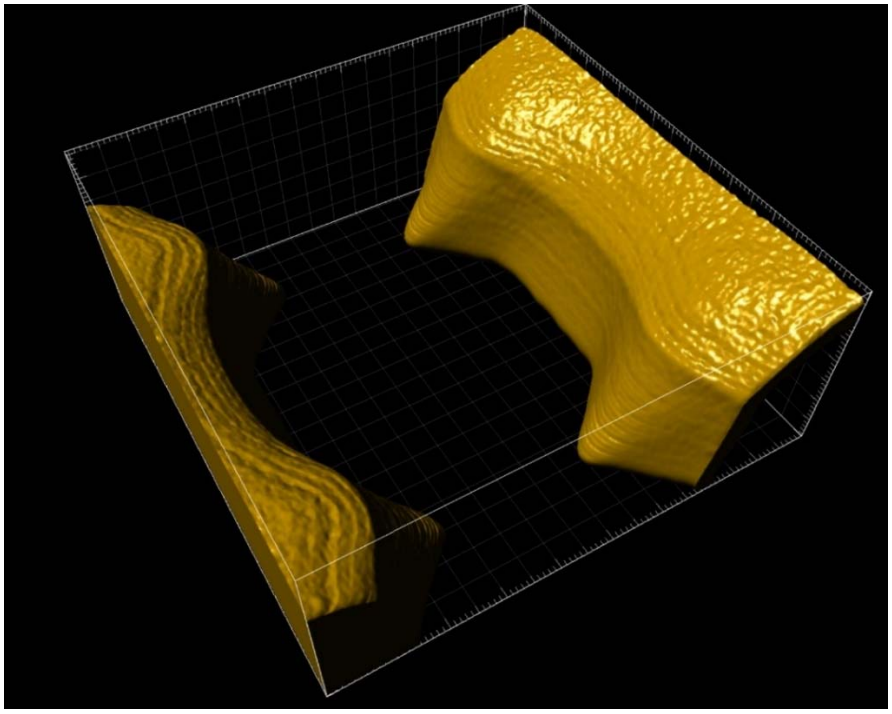

Figure 4.2 3-D fluorescent imaged of 3-D microfunnels filled with 1 mM FITC solution.

4.2 Characterization of nanofluidic properties

1mM KCl solution was prepared in deionized water. PDMS channel sample was bonded to the glass by oxygen plasma treatment and immediately filled with KCl solution by the capillary force. The current was measured by the electrometer from Keithley (6517B) with 1mM KCl solution in the deionized water. After two electrodes were placed in the reservoirs, DC voltage was applied from 0 V to 50 V with 0.05 mV/sec step voltage. Keithley software program was used to control the parameters and analysis.

Figure 4.3 Experimental setup to measure I-V characteristics of mixed-scale PDMS channel network; (Left) an electrometer, (Right) a faraday cage to block noise signal from outside.

The result of the experiment is shown by Figure 4.4. The first blue region is the ohmic current region from 0 V to 9 V. This part is that current is gradually increased with voltage increase by ohmic behavior. The second pink region is the limiting current region. In the limiting current part, the current increase followed by the voltage increase is limited because ion depletion region is formed around the nanochannel and then current increase is almost slow. The final green part is the overlimiting current region. In the overlimiting region, current through the nanochannel increases once again. Overlimiting current is occurred owing to continuously increased voltage. Therefore, nanofluidics properties were characterized through the experiment of the current measurement.

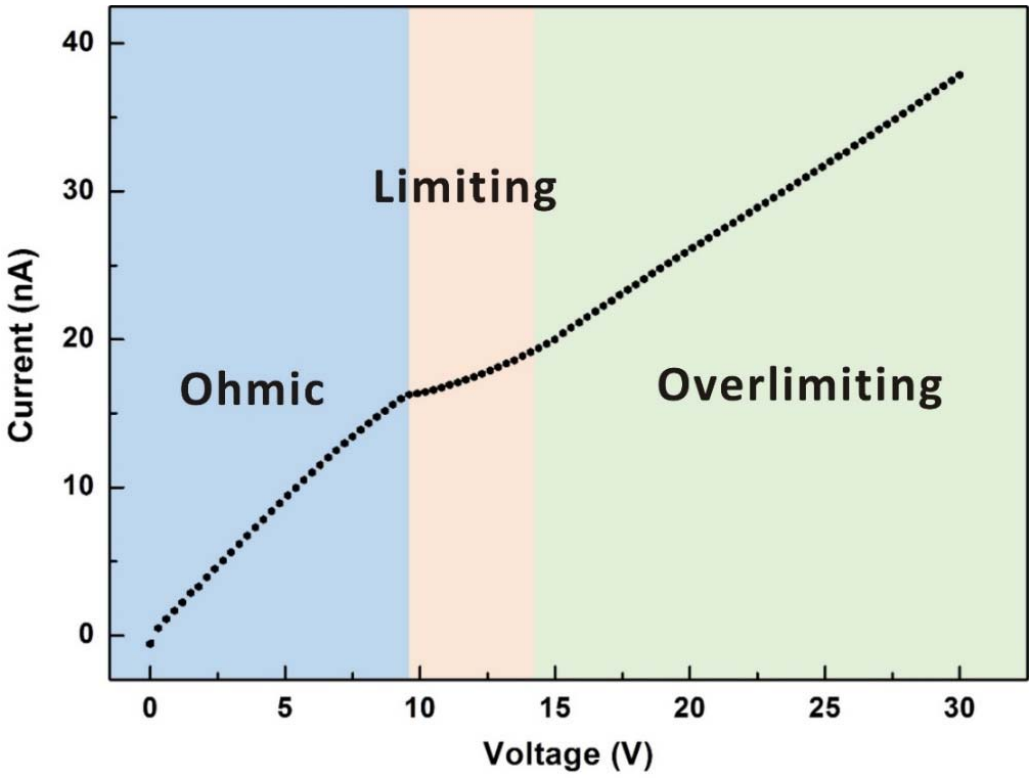

Figure 4.4 I-V characteristic curve of a mixed-scale PDMS channel network. The curve contains Ohmic current region (0V ~ 9V), limiting current region (9V ~ 14V) and overlimiting current region (>14V).

4.3 Micro-particle entrapment

4.3.1 Background

Electroporation is the efficient technology for the transfection that biomolecules such as a DNA, a plasmid, and a protein are efficiently delivered into the cell [18-20]. There are several electroporation methods including the bulk electroporation (BEP) in bulk condition, microchannel electroporation (MEP) and nanoelectroporation (NEP) using the microchannel or the nanochannel. BEP technology has been applied generally using the commercial equipment but their efficiency is remarkably lower than MEP or NEP. Efficiency and precise of the delivery are crucial for the electroporation. So MEP or NEP have been developed by several research groups and applied for the precise controlled electroporation using the phenomenon that the electric field across the channels is focused to the narrow channel with biomolecule surface. In this sense, NEP is the most efficient technology for the electroporation. But complex, high cost and long fabrication process have obstructed a broad NEP research. In this chapter, the mixed-scale PDMS channel networks will be applied to trap the micro particle in the 3-D microfunnels to show the functionality as a NEP platform. The mixed-scale PDMS channel networks will provide various advantages for the NEP such as easy, cost effective, mass productive fabrication process and high efficient and precise electroporation. A gradually tapered 3-D microfunnel structures will efficiently trap the single particle. Finally, the most valuable structure for the electroporation can be optimized through the freely controllable funnel inlet angles, nose lengths, channel thicknesses and shapes. Also, various 3-D microfunnels including the various inlet angles and nose lengths were used to optimize the best structure in this experiment.

4.3.2 Experimental

1-μm microparticles were scattered by the sonication to obstruct their settle before the dilution and diluted by 1-μL in 1-mL DI water. The mixed-scale PDMS channel networks samples with 30^{o}, 60^{o}, 90^{o} and 120^{o} 3-D micofunnels including 5-μm, 10-μm and 15-μm heights were used to optimize the superb funnel structure for the single microparticle trap. PDMS channel sample was bonded to the glass substrate by the oxygen plasma treatment and filled with the diluted microparticle solution by the capillary force. When two platinum electrodes were soaked into the two reservoirs of the PDMS, AC voltage was applied from 10V to 100V to optimize the proper voltage. The movements of the microparticles were inspected by the inverted microscope.

.

4.3.3 Results

Microfunnel structure was defined as funnel nose length and funnel inlet angle shown by Figure 4.5. The mixed-scale PDMS channels with 3D-funnel structure including nose lengths of 5-μm, 10-μm, 15-μm and inlet angles of 30°, 60°, 90°, 120° were used to the particle entrapment experiment. Figure 4.6 is SEM images of top-view of the SU-8 photoresist funnel structures and pyrolyzed carbon funnel structures with various inlet angles and nose lengths. Figure 4.6 confirms that 12 sets of the microfunnels were successfully patterned to the SU-8 photoresist during the 2-steps UV lithography process and various inlet angles and nose lengths were maintained as designed patterns intactly. Meanwhile, approximately 1-μm mismatch was occurred during the alignment between the thin SU-8 structure and thick SU-8 structure.

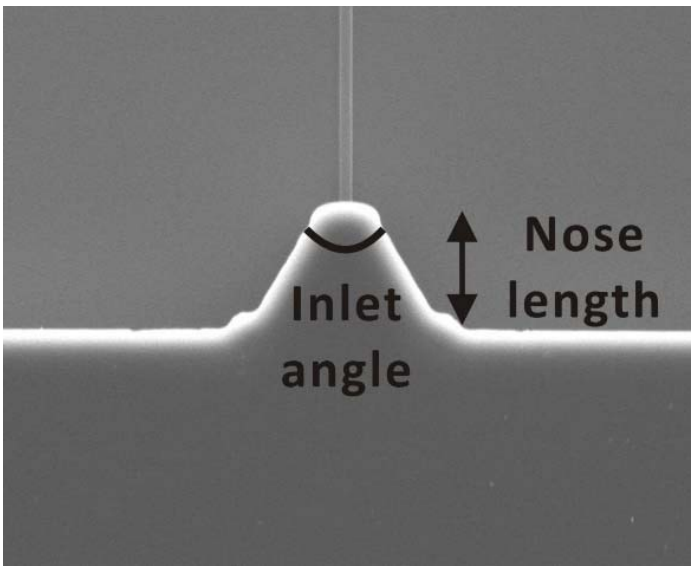

Figure 4.5 SEM images of the top-view of the SU-8 photoresist structure. Microfunnel structure was defined as funnel inlet angle including 30°, 60°, 90° and 120° and funnel nose length including 5-μm, 10-μm and 15-μm.

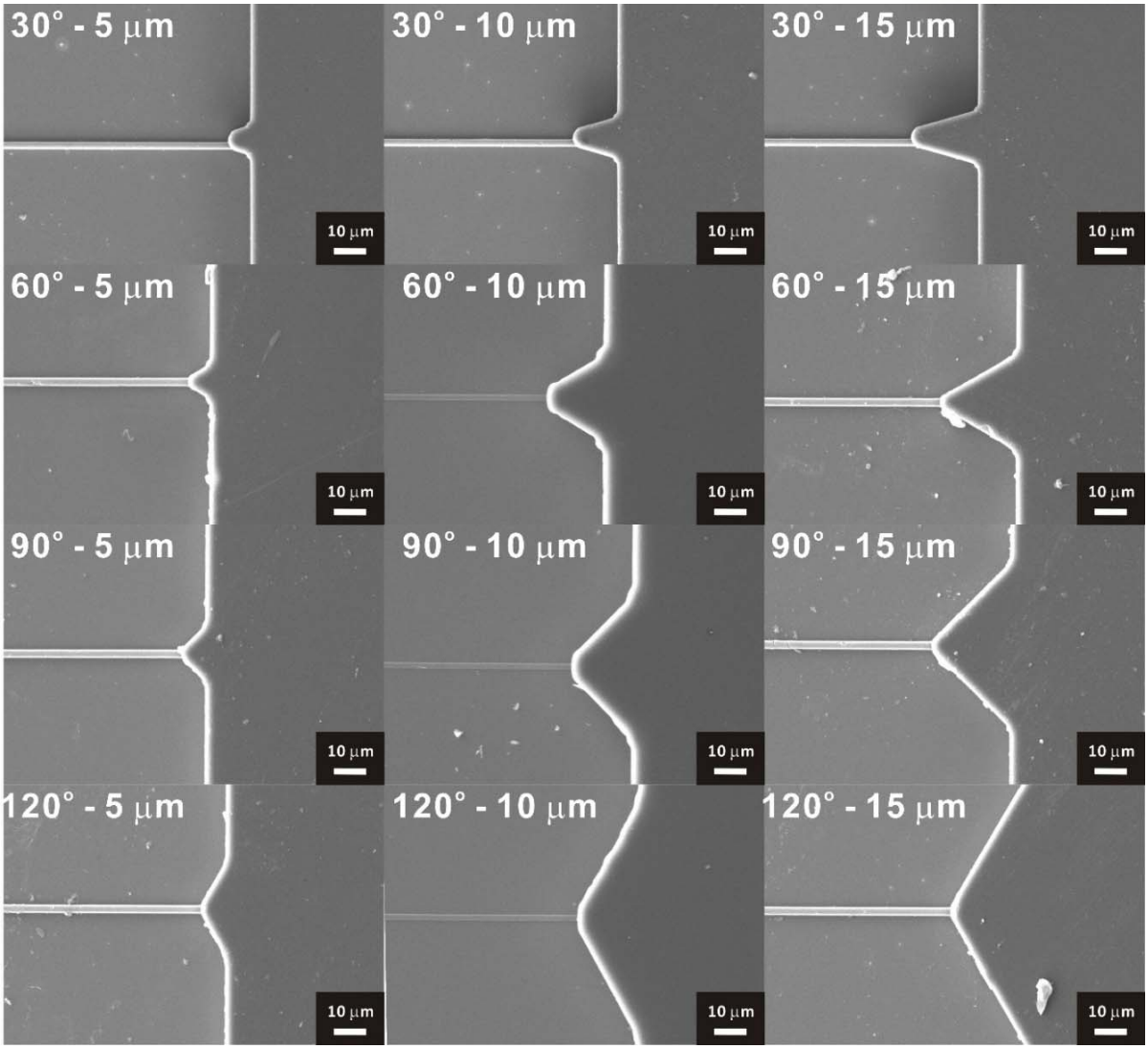

Figure 4.6 SEM images of the top-view of the SU-8 photoresist 3-D microfunnel structures. SU-8 photoresist structures were successfully transferred with inlet angles of 30º, 60º, 120º and nose lengths of 5-μm, 10-μm, and 15-μm during the UV lithography.

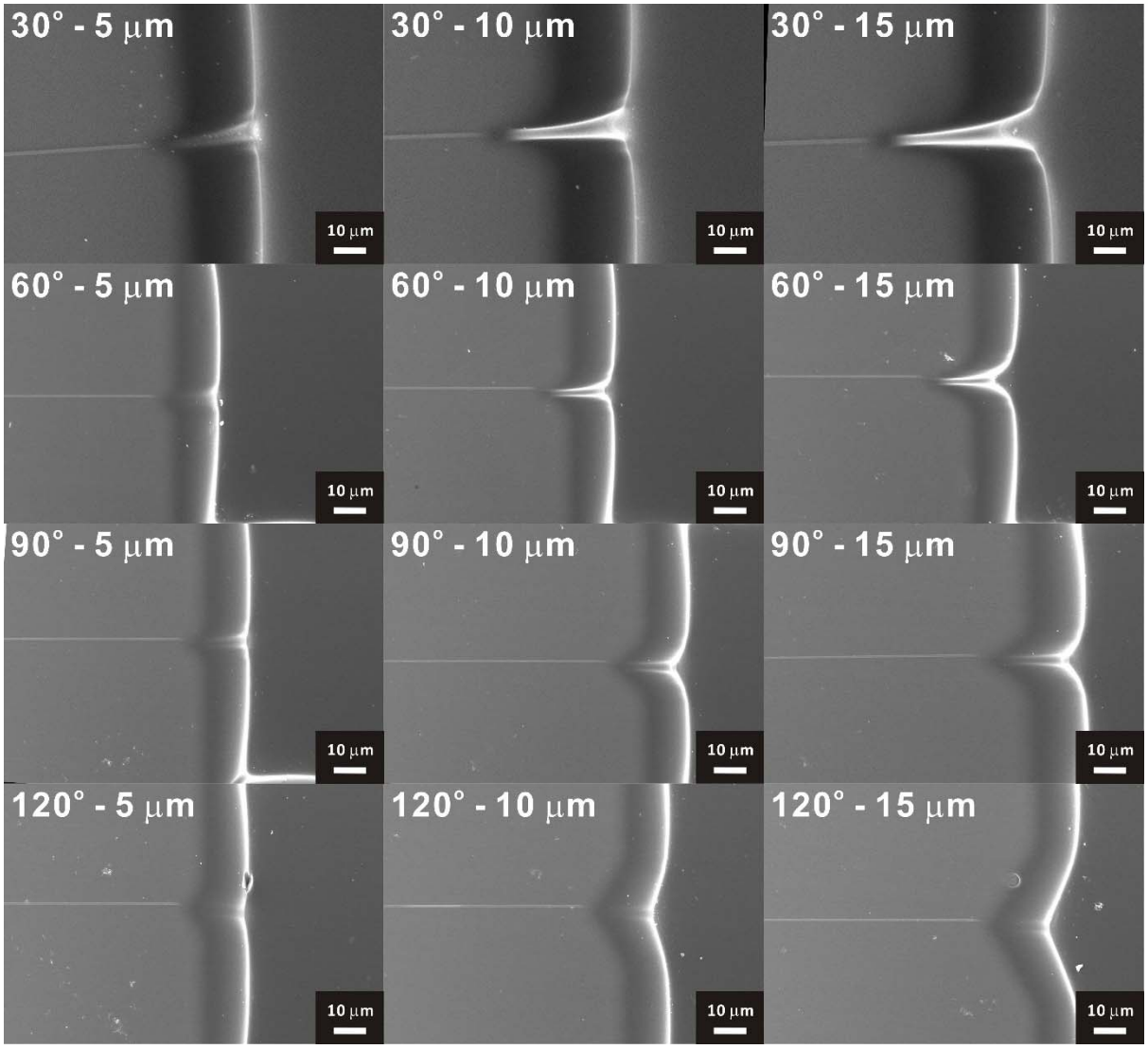

Figure 4.7 SEM images of the top-view of the carbon structure with 3D-funnel structures. Pyrolyzed carbon structures were successfully converted with inlet angles of 30º, 60 º, 120 º and nose lengths of 5-μm, 10-μm, and 15-μm during the pyrolysis process.

SEM images show the 12 sets of the 3-D microfunnels including the various inlet angles and nose lengths of the pyrolyzed carbon structure after the pyrolysis process shown by Figure 4.7. All 3-D microfunnels were successfully converted to the pyrolyzed carbon structures without any deformation. After the pyrolysis process, various inlet angles were maintained all nose lengths were decreased due to the volume shrinkage. Despite the mismatch after the 2-steps UV lithography process, mixed-scale carbon structures were smoothly connected between nanostructure and microstructure without the break. Figure 4.8 describes the SEM images of the SU-8 structure (a), pyrolyzed carbon structure (b) and schematic images of the pyrolyzed carbon structure (c), single microparticle trapped in the PDMS 3-D microfunnel.

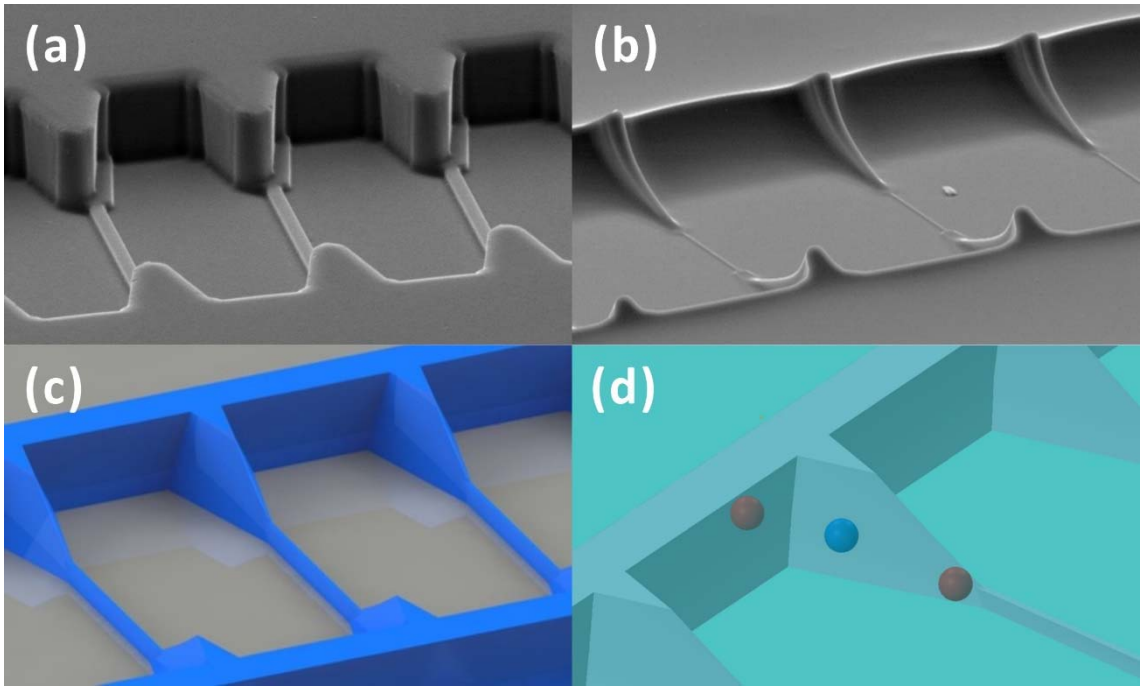

Figure 4.8 Images of the 3-D funnel structures. (a) SEM image of SU-8 structures before pyrolysis and (b) pyrolyzed carbon structures. (c) Schematic image of the pyrolyzed carbon structure and (d) a 3-D PDMS funnel trapping a single micro particle.

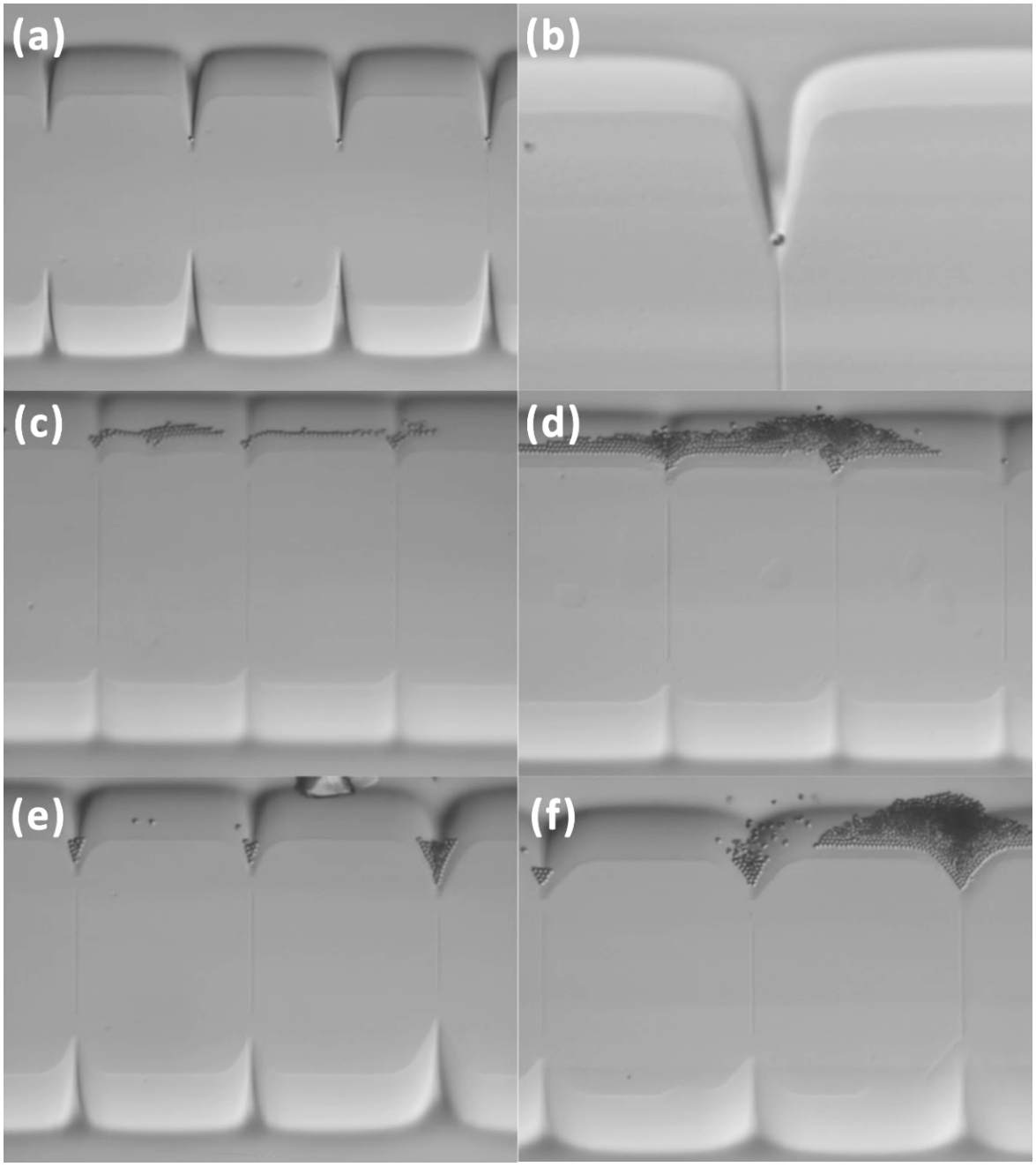

Figure 4.9 Optical microscopy images of the mixed-scale PDMS channel network including 3-D funnels, micro-nanochannels, nanochannels and trapped 1-μm-diameter micro particles. (a-b) Single entrapment of micro particles with microfunnels with 30^{o} of entrance angle and 15μm in height. (c-f) Entrapment of multiple micro particles at 3-D funnels with wide and short entrance.

The solution including 1-μm microparticles was flowed to the mixed-scale PDMS channel networks from the reservoirs. Negatively charged 1-μm microparticles were moved from the cathode to the anode using applied voltage 30V by the electrophoresis. Figure 4.9 shows the optical microscopic images of the trapped microparticles at the inlet of the various 3-D microfunnels. (a)-(b) are single trapped microparticles. Particularly, 30^{o} microfunnels with 5-μm, 10-μm and 15-μm heights were the most efficient structures to trap the single microparticle. Because small void of the narrow inlet angle helps the capture of the single microparticle. (c) is floating microparticles without single capture. (d)-(f) are overly trapped microparticles at the wide inlet microfunnels. Dozens of 1-μm particles were trapped at wider inlet angle microfunnels such as 60^{o}, 90^{o}, 120^{o} because of the large void area at the inlet of the 3D-funnel and lacking focus of the electric field on the nanochannel. Table 3. shows the overall results of the particle trap. Particle trap and efficient 3-D microfunnel structures were demonstrated and optimized through this experiment. This experiment demonstrates that the microfunnels including the narrow inlet angle are the best structure for single particle trap, the microfunnels including the wide inlet angle trap dozens of the microparticles and the microfunnels with short nose length cannot trap the microparticles.

Table 2. Table of the listed 3-D microfunnel structures and success and failure of the particle entrapment. Microparticle entrapments succeeded in inlet angle 30º microfunnel with 10-μm and 15-μm nose lengths.

Funnel inlet angle	Funnel nose length	Trap or Failure
30º	5-μm	Failure
30º	10-μm	Trap
30º	15-μm	Trap
60º	5-μm	Failure
60º	10-μm	Failure
60º	15-μm	Failure
90º	5-μm	Failure
90º	10-μm	Failure
90º	15-μm	Failure
120º	5-μm	Failure
120º	10-μm	Failure
120º	15-μm	Failure

5

Conclusions

Finally, conclusion of this thesis will be recapitulated in this chapter.

5. Conclusions

In this thesis, mixed-scale PDMS channel networks were successively fabricated using soft lithography and carbon-MEMS that consists of UV lithography and pyrolysis processes. Thin polymer micro structures (width = 1.1 μm, thickness = 330 nm, length = 100 μm) could be converted into carbon nanostructures (width = 441 nm, thickness = 55 nm, length = 121 μm) during the pyrolysis process because of an enormous volume shrinkage. The enormous volume shrinkage during pyrolysis enabled the formation of convex mixed-scale monolithic carbon molds with 3D-micro funnels. Also, the shape and dimensions of mixed-scale carbon structure could be easily controlled by changing photomask design and photoresist thickness. The inclined side wall and hydrophobic surface enabled efficient PDMS demolding process and thus the carbon mold could be reused more than 40 times. Surface free energy of the carbon was changed correspondingly to the pyrolysis temperature. The functionality of the mixed-scale PDMS channel was evaluated using the fluorescence imaging, current measurement and micro-particle entrapment. Fluorescence imaging proved the hermetic sealing and uniformity of the PDMS nanochannels. Single micro-particle could be trapped at the junction of a nanochannel and a microchannel owing to the 3-D microfunnel structure. Therefore, the mixed-scale PDMS channel network is expected to be applied to nanoelectroporation for effective cell transfection.

REFERENCES

[1] J. M. Perry, K. Zhou, Z. D. Harms, and S. C. Jacobson, "Ion transport in nanofluidic funnels", *ACS Nano*, vol. 4, pp. 3897-3902 (2010).

[2] B. Kim, J. Heo, H. J. Kwon, S. J. Cho, J. Han, S. J. Kim, and G. Lim, "Tunable ionic transport for a triangular nanochannel in a polymeric nanofluidic system", *ACS Nano*, vol. 7, pp. 740-747 (2013).

[3] S. J. Kim, Y. C. Wang, J. H. Lee, H. Jang, and J. Han, "Concentration polarization and nonlinear electrokinetic flow near a nanofluidic channel", *Phys. Rev. Lett.,* vol. 99, pp. 044501 (2007).

[4] J. W. Honschoten, N. Brunets, and N. R. Tas, "Capillarity at the nanoscale", *Chem. Soc. Rev.*, vol. 39, pp. 1096-1114 (2010).

[5] H. Daiguji, "Ion transport in nanofluidic channels", *Chem. Soc. Rev.*, vol. 39, pp. 901-911 (2010).

[6] S. J. Kim, S. H. Ko, K. H. Kang, and J. Han, "Direct seawater desalination by ion concentration polarization", *Nat. Nanotechnol.* , vol. 21, pp. 297-301 (2010).

[7] L. J. Cheng, and L. J. Guo, "Nanofluidic diodes", *Chem. Soc. Rev.*, vol. 39, pp. 923-938 (2010).

[8] S. Chung, J. H. Lee, M. W. Moon, J. Han, and R. D. Kamm, "Non-lithographic wrinkle nanochannels for protein preconcentration", *Adv. Mater.*, vol. 20, pp. 3011-3016 (2008).

[9] A. Syed, L. Mangano, P. Mao, J. Han, and Y. A. Song, "Creating sub-50 nm nanofluidic junctions in a PDMS microchip via self-assembly process of colloidal silica beads for electrokinetic concentration of biomolecules", *Lab Chip*, vol. 14, pp. 4455-4460 (2014).

[10] J. H. Lee, B. D. Cosgrove, D. A. Lauffenburger, and J. Han, "Microfluidic concentration-enhanced cellular kinase activity assay", *J. Am. Chem. Soc.*, vol. 131, pp. 10340-10341 (2009).

[11] A. E. Muniz, and A. Merkoci, "A nanochannel/ nanoparticle-based filtering and sensing platform for direct detection of a cancer biomarker in blood", *Small*, vol. 7, pp. 675-682 (2011).

[12] Y. Koh, H. Kang, S. H. Lee, J. K. Yang, J. H. Kim, Y. S. Lee, and Y. K. Kim, "Nanoslit membrane-integrated fluidic chip for protein detection based on size-dependent particle trapping", *Lab Chip*, vol. 14, pp. 237-243 (2014)

[13] S. Lee, Y. Kim, M. Park, H. S. Park, S. Cho, J. H. Cho, J. Park, and W. Hwang, "Nanoporous membrane for immunoprotection biofilter", *18th International Conference on Composite Materials*.

[14] Y. C. Wang, A. L. Stevens, and J. Han, "Million-fold preconcentration of proteins and peptides by nanofluidic filter", *Anal. Chem.*, vol. 77, pp. 4293-4299 (2005).

[15] Y. Kim, K. S. Kim, K. L. Kounovsky, R. Chang, G. Y. Jung, J. J. Pablo, K. Jo, and D. C. Schwartz, "Nanochannel confinement: DNA stretch approaching full contour length", *Lab Chip*, vol. 11, pp. 1721-1729 (2011).

[16] F. I. Uba, S. R. Pullagurla, N. Sirasunthorn, J. Wu, S. Park, R. Chantiwas, Y. K. Cho, H. Shin, and S. A. Soper, "Surface charge, electroosmotic flow and DNA extension in chemically modified thermoplastic nanoslits and nanochannels", *Analyst,* vol. 140, pp. 113-126 (20105).

[17] B. C. Kim, C. Moraes, J. Huang, M.C. Thouless, and S. Takayama, "Fracture-based micro- and nanofabrication for biological applications", *Biomater. Sci.*, vol. 2, pp. 288-

296 (2014).

[18] P. E. Boukany. A. Morss, W.C. Liao, B. Henslee, H. Jung, X. Zhang, B. Yu, X. Wang, Y. Wu, L. Li, K. Gao, X. Hu, X. Zhao, O. Hemminger, W. Lu, G. P. Lafyatis, and L. J. Lee, "Nanochannel electroporation delivers precise amounts of biomolecules into living cells", *Nat. Nanotechnol.*, vol. 6, pp. 747-754 (2011).

[19] K. Gao, L. Li, L. He, K. Hinkle, Y. Wu, J. Ma, L. Chang, X. Zhao, D. G. Perez, S. Eckardt, J. Mclaughlin, B. Liu, D. F. Farson, and L. J. Lee, "Design of a microchannel-nanochannel-microchannel array based nanoelectroporation system for precise gene transfection", *Small*, vol. 10 pp. 1015-1023 (2014).

[20] S. Wang, and L. J. Lee, "Micro-/nanofluidics based cell electroporation", *Biomicrofluidics*, vol. 7, pp. 011301 (2013).

[21] F. Persson, J. Fritzsche, K. U. Mir, M. Modesti, F. Westerlund, and J. O. Tegenfeldt, "Lipid-based passivation in nanofluidics", *Nano Lett.*, vol. 12, pp. 2260-2265 (2012).

[22] S. H. Kim, Y. Cui, M. J. Lee, S. W. Nam, D. Oh, S. H. Kang, Y. S. Kim, and S. Park, "Simple fabrication of hydrophilic nanochannels using the chemical bonding between activated ultrathin PDMS layer and cover glass by oxygen plasma", *Lab Chip*, vol. 11, pp. 348-353 (2011).

[23] R. Yokokawa, Y. Yoshida, S. Takeuchi, T. Kon, and H. Fugita, "Undirectional transport of a bead on a single mictotubule immobilized in a submicrometre channel", *Nanotechnology*, vol. 17, pp. 289-294 (2006).

[24] L. D. Menard, and J. M. Ramsey, "Fabrication of sub-5 nm nanochannels in insulating substrates using focused ion beam milling", *Nano Lett.*, vol. 11, pp. 512-517 (2011).

[25] N. Yao, and A. K. Epstein, "Surface nanofabrication using focused ion beam", *Microscopy: Science, Technology, Application and Education*, pp. 2190-2199(2010).

[26] R. Chantiwas, M. L. Hupert, S. R. Pullagurla, S. Balamurugan, J. T. Lopez, S. Park, P. Datta, J. Goettert,k Y. K. Cho, and S. A. Soper, "Simple replication methods for producing nanoslits in thermoplastics and the transport dynamics of double-stranded DNA through these slits", *Lab Chip*, vol. 10, pp. 3255-3264, (2010).

[27] J. Wu, R. Chantiwas, A. Amirasadeghi, S. A. Soper, and S. Park, "Complete plastic nanofluidic devices for DNA analysis via direct imprinting with polymer stamps", *Lab Chip*, vol. 11, pp. 2984-2989 (2011).

[28] L. H. Thamdrup, A. Klukowska, and A. Kristensen, "Stretching DNA in polymer nanochannels fabricated by thermal imprint in PMMA", *Nanotechnology*, vol. 19, pp. 125301 (2008).

[29] V. N. Truskett, and M. P. C. Watts, "Trends in imprint lithography for biological applications", *Trends Biotechnol.*, vol. 24, pp. 312-317 (2006).

[30] C. Duan, W. Wang, and Q. Xie, "Fabrication of nanofluidic devices", *Biomicrofluidics*, vol. 7, pp. 026501 (2013).

[31] Z. Yin, E. Cheng, and H. Zou, "A nobel hybrid patterning technique for micro and nanochannel fabrication by integrating hot embossing and inverse UV lithography", *Lab Chip*, vol. 14, pp. 1614-1621 (2014).

[32] S. Azimi, Z. Dang, C. Zhang, J. Song, M. B. H. Breese, C. H. Sow, J. A. Kan, and J. R. C. Maarel, "Buried centimeter-long micro- and nanochannel arrays in porous silicon and glass", *Lab Chip*, vol. 14, pp. 2081-2089 (2014).

[33] H. Schmid, and B. Michel, "Siloxane Polymers for High-Resolution, High-accuracy soft lithography", *Macromolecules*, vol. 33, pp. 3042-3049 (2000).

[34] T. W. Odom, J. C. Love, D. B. Wolfe, K. E. Paul, and G. M. Whitesides, "Improved pattern transfer in soft lithography using composite stamps", *Langmuir*, vol. 18, pp. 5314-5320 (2002).

[35] R. Chantiwas, S. Park, S. A. Soper, C. H. Kim, S. Takayama, V. Sunkara, H. Hwang, and Y. K. Cho, "Flexible fabrication and applications of polymer nanochannels and nanoslits", *Chem. Soc. Rev.*, vol. 40, pp. 3677-3702 (2011).

[36] S. M. Park, Y. S. Huh, H. G. Craighead, and D. Erickson, "A method for nanofluidic device prototyping using elastomeric collapse", *Proc. Nat. Acad. Sci. USA*, vol. 106, pp. 155549-15554 (2009).

[37] L. M. Bellan, E. A. Strychalski, H. G. Craighead, "Nanochannels fabricated in polydimethylsiloxane using sacrificial electrospun polyethylene oxide nanofibers", *J. Vac. Sci. Technol. B*, vol. 26, pp. 1728-1731 (2008).

[38] J. Heo, H. J. Kwon, H. Jeon, B. Kim, S. J. Kim and G. Lim, "Ultra-high-aspect-orthogonal and tunable three dimensional polymeric nanochannel stack array for BioMEMS applications", *Nanoscale*, vol. 6, pp. 9681-9688 (2014)

[39] D. Huh, K. L. Mills, X. Zhu, M. A. Burns, M. D. Thouless, and S. Takayama, "Tuneable elastomeric nanochannels for nanofluidic manipulation", *Nat. Mater.*, vol. 6, pp. 424-428 (2007).

[40] J. I. Heo, D. S. Shim, G. T. Teixidoe, S. Oh, M. J. Madou, and H. Shin, "Carbon interdigitated array nanoelectrodes for electrochemical applications", *J. Electrochem. Soc.*, vol. 158 (3), pp. J76-J80 (2011).

[41] Y. Lim, J. I. Heo, M. Madou, and H. Shin, "Monolithic carbon structures including suspended single nanowires and nanomeshes as a sensor platform", *Nanoscale Res. Lett.*, vol. 8, pp. 492 (2013).

[42] Y. Lim, J. I. Heo, and H. Shin, "Fabrication and application of a stacked carbon electrode set including a suspended mesh made of nanowires and a substrate-bound planar electrode toward for and electrochemical/ biosensor platform", *Sensors and actuator B: chemical*, vol. 192, pp. 796-803 (2014).

[43] L. Yang, N. Shirahata, G. Saini, F. Zhang, L. Pei, M. C. Asplund, D. G. Kurth, K. Ariga, K. Sautter, T. Nakanishi, V. Smentkowski, and M. R. Linford, "Effect surface free energy on PDMS transfer in microcontact printing and its applications to TOF-SIMS to probe surface energies", *Langmuir*, vol. 25, pp. 5674-5683 (2009).

[44] M. J. Lee, N. Y. Lee, J. R. Lim, J. B. Kim, M. Kim, H. K. Baik, and Y. S. Kim, "Antiadhesion surface Treatments of molds for High-Resolution Unconventional Lithography", *Adv. Mater.*, vol. 18, pp. 3115-3119 (2006).

[45] D. K. Owens, and R. C. Wendt, "Estimation of the surface free energy of polymers", *J. Appl. Polym. Sci.*, vol. 13, pp. 1741-1747 (1969).

ACKNOWLEDGEMENTS

I am deeply indebted to my advisor, Professor Heungjoo Shin, who gave many opportunities for various experiences, excellent guidance and caring. He continually and convincingly conveyed a spirit of research and a wisdom of life. Also, He advised spiritually for concern. Without his guidance and persistent help, this thesis would not have been possible.

I would like to express the appreciation to the committee members, Professor Taesung Kim and Professor Jaesung Jang for giving their wise words, suggestion and assistance during the preparation with this thesis. Thanks to them, I could successfully complete this thesis.

My special thanks go to my Lab colleagues, Dr. Deepti Sharma, Yeongjin Lim, Jongmin Lee and Junyeong Seo, for helping and encouraging throughout my master course. Dr. Deepti Sharma gave advice and encouragement like my elder sister. Yeongjin Lim gave support, discussion and inspiration for my experiments throughout the master course. Also, I would like to thank junior colleagues, Jongmin Lee and Junyeong Seo, for giving their encouragement, joy and kindness. Thanks to them, I could enjoy research and study anytime without loneliness.

I would like to extend special thanks to “The Microfluidics/ Nanomechanics (μFNM) Lab” members. Minseok Kim, Jiwon Alex Lim, Hyunmoon Nam, Jongwan Lee and Dokgyeong Ha gave countless helps and suggestions for experiments and life in Ulsan. Also, they generously teach and lend their devices including oxygen plasma, spin-coater and microscope. Also, I am grateful to Hoon Yi for helping measurement of adhesion force in “Multiscale Biomimetics and Manufacturing (MBM) Lab”.

I would like to express the appreciation to UCRF members for their effort into great management of the devices, kindness and training for self-user. Especially, Jin-Hoe Hur gave a deep understanding and various helps including teaching and operating the microscope for imaging experiment.

For my friends, I would like to thank to Kyeongmi Kim, Misuk Kim, Buyeong Kim, Seonwoo Choi, Donghyeon Cho and Woobean Lee for their constant friendship and encouragement from the spring of 2008.

Finally but most importantly, I would like to express the deepest appreciation to my family. My parents, Seungyeon Lee and Geumok Seo gave birth, their support and encouragement both physically and spiritually throughout my life. They has always supported and waited for my choices and new challenges. Also, I wish to thank to my elder sister and her husband, Jiyeong Lee and Jeongho An, my younger brother, David Jeong-il Lee and my lovely nephew and niece, Seohyun An and Seoyoung An for giving a lot of joy, encouragement and inspiration always by my side.